Journal of Physical and Theoretical Chemistry
of Islamic Azad University of Iran, 15 (1) 47-78: Spring 2018
(J. Phys. Theor. Chem. IAU Iran)
ISSN 1735-2126

TD-DFT Calculations, Electronic Structure, Biological Activity, NBO , NLO Analysis and Electronic Absorption Spectra of Some 3-formyl Chromone Derivatives

Shimaa A. H. Heussein[2,*], H. Moustafa[1], Nabil H. Amin[2], Magdy Ahmed[2] and ELShimaa Ibrahim[2]

[1] Department of Chemistry, Faculty of Science, Cairo University, Giza, Egypt
[2] Department of Chemistry, Faculty of Education, Ain Shams University, Roxy 11711, Cairo, Egypt

Received August 2018; Accepted October 2018

ABSTRACT

The electronic structure and spectra of 3-formyl Chromone and some of its derivatives are investigated using TD-DFT/B3LYB/6-311G (d, p) level of theory. The results of calculations show that all the studied compounds **1–6** are planar, as indicated from the dihedral angles. The electronic absorption spectra of the studied compounds are recorded in the UV-VIS region, in both ethanol (as polar solvent) and dioxane (as non-polar solvent). The observed vertical electronic transitions assignments are facilitated via time-dependent density functional theory TD-DFT. The theoretical spectra computed at CAM-B3LYP/6-311G (d, p) in gas phase, ethanol and dioxane nicely reproduce the observed spectra. The natural bond orbital (NBO) analysis were discussed in terms of the extent of delocalization, intermolecular charge transfer and second order perturbation interactions between donor and acceptor MOs. The calculated E_{HOMO} and E_{LUMO} energies of the studied compounds can be used to explain the extent of charge transfer in the molecule and to calculate the global properties; the chemical hardness (η), global softness (S), electrophilicity (ω), and electronegativity (χ). The calculated nonlinear optical parameters (NLO); polarizibilty (α), anisotropy of the polarizibility ($\Delta\alpha$) and first order hyperpolarizibility (β) of the studied compounds have been calculated at the same level of theory and compared with the proto type Para-Nitro-Aniline (PNA), show promising optical properties. 3D-plots of the molecular electrostatic potential (MEP) for some of the studied compounds are investigated and analyzed showing the distribution of electronic density of orbital's describing the electrophilic and nucleophilic sites of the selected molecules. The biological activity of the studied compounds was tested against gram positive, gram negative and Fungi.

Keywords: UV spectra; TD-DFT; NBO and NLO analysis; biological activity; 3-formyl Chromone derivatives.

INTRODUCTION

Chromones are well known natural and synthetic products that possess diverse biological activities [1], including anticancer [2-4], antitumor [5], antiproliferative [6], neuroprotective [7], HIV-inhibitory [8,9], antimicrobial [10,11], antioxidant [12], anti-inflammatory [13], and antibiotic [14]. Heteroannulated chromones showed significant biological activity including pharmacological [15], antiplatelet [16], antiallergic [17], antiangiogenic [18],

* Corresponding author: Shimaaquantum@ymail.com

antirheumatic [19], antibacterial [20], anti-inflammatory and analgesic [21]. Friedländer condensation of 2-aminochromone-3-carboxaldehydes is a well-known reaction for preparation of chromeno[2,3-b]pyridine derivatives [22-25].

The electronic absorption and emission spectra manifests the electronic structure and spectra of molecules. theses according to understanding of the forces that govern the electronic structure of the proposed molecules. Now there is no systematic study of substituent and solvent effects on the observed spectra of 3-fromyl-chromone. Such a study is very important in understanding their electronic structure which may correlate with their biological activity.

The newly synthesized compounds 3-fromyl-chromone derivatives **1-6** are expected to have biological potential which needs to be explored by investigating their electronic structure and spectra experimentally and theoretically. The UV spectra, NLO and NBO analysis have been used to explain charge transfer within these molecules. The solvatochromism PCM is dependence of the electronic transitions of these molecules on the polarity of the solvent can be inferred from solvent-induced changes of such transitions.

In the literature there is no systematic study of the electronic structure, substituent effect and bonding characteristics of the studied compounds. Therefore, our contribution in previous work [26-28], is to shed more light on the geometrical parameters (bond lengths, bond angles and dihedral angles), ground state properties of the 3-fromyl-chromone derivatives energy gaps (highest occupied molecular orbital [HOMO]–lowest unoccupied molecular orbital [LUMO]), Natural charges, effect of substituent's of different electron donating-withdrawing power in the one aryl moiety, and electrostatic potential are calculated using B3LYP/6-311G (d,p). The electronic dipole moment (μ), and first order hyperpolarizibility (β) values of the studied compounds have been computed to study the NLO properties to identify and characterize the forces that govern the structure-activity and the optical properties of the studied compounds. Finally, global reactivity descriptors including electronegativity (X), hardness (η), softness (S), and electrophilicity ***(ω)*** of the studied compounds were calculated and analyzed, while molecular electrostatic potential (MEP) of molecules were explored as well.

The present work attempts to provide a detailed experimental (UV) using TD-DFT and theoretical electronic structure 3-fromyl-chromone derivatives using CAM-B3LYP/6-311G (d, p). Also; studied the structure activity relationship (SAR) by using the antimicrobial activity application for the compounds **1-6**. The contributing configurations and MOs are characterized by the origin of each absorption band. The charge transfer of the electron density in the studied molecular systems are characterized by natural bond orbital analysis (NBO) and identify the extent of delocalization of conjugative interaction between different subsystems of the studied compounds. The effect of solvent polarity on the observed spectra and hence, predicting the relative stabilities, extent of charge transfers character and assignment of the observed electronic transitions are analyzed. The effect substituent's of different electron donating group (X=CH3) and electron withdrawing groups (X= Br and Cl) on the electronic spectra of the studied compounds are discussed and analyzed.

EXPERIMENTAL COMPOUNDS

The structure of the six proposed

molecules **1–6** of 3-fromyl-chromone derivatives, is shown below, where compound **1** is chromone-3-carboxaldehyde, compound **2** is 6-methylchromone-3-carboxaldehyde, compound **3** is 6,8-dimethylchromone-3-carboxaldehyde, compound **4** is 6-bromochromone-3-carboxaldehyde, compound **5** is 6-chlorochromone-3-carboxaldehyde, and compound **6** is 6,8-dichlorochromone-3-carboxaldehyde.

Compounds	X	Y
1	H	H
2	CH_3	H
3	CH_3	CH_3
4	Br	H
5	Cl	H
6	Cl	Cl

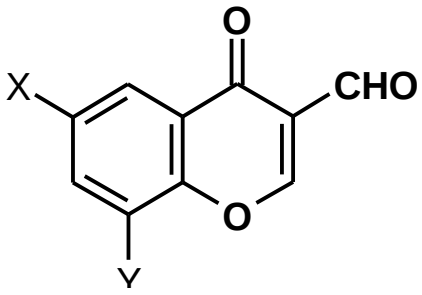

Solvents

Polar (ethanol) and non-polar (dioxane) solvents were obtained from Merck, AR-grade, and were used without further purification.

Apparatus

A Perkin Elmer lambda 4B spectrophotometer using 1.0 cm fused quartz cells were used to measured the electronic absorption spectra over the range 200-900 nm.

Antimicrobial Study

Biological activities of synthesized 3-fromyl-chromone derivatives compounds were studied for antibacterial and antifungal properties against different types of bacteria; Gram positive S. aureus, and B. subtillis and Gram-negative E. coli (Escherichia coli) and S. typhimurium, and C. albicans and A. fumigates for fungus.

Computational details

All computations were carried out using Khon-Sham's DFT method subjected to the gradient-corrected hybrid density functional B3LYP method [29]. This function is a combination of the Becke's three parameters non-local exchange potential with the non-local correlation functional of Lee et al [30]. For each structure, a full geometry optimization was performed using this function [30] and the 6-311G (d, p) bases set [31] as implemented by Gaussian 09 package [32]. All geometries were visualized either using Gauss View 5.0.9 [33] or chemcraft 1.6 [34] software packages. No symmetry constrains were applied during the geometry optimization. Also, the total static dipole moment (μ), $\langle\Delta\alpha\rangle$, and $\langle\beta\rangle$, values were calculated by using the following equations [35-37]:

$$\mu = (\mu^2_x + \mu^2_y + \mu^2_z)^{1/2},$$
$$\langle\alpha\rangle = 1/3\,(\alpha_{xx} + \alpha_{yy} + \alpha_{zz}),$$
$$\Delta\alpha = ((\alpha_{xx} - \alpha_{yy})^2 + (\alpha_{yy} - \alpha_{zz})^2 + (\alpha_{zz} - \alpha_{xx})^2/2)^{1/2},$$
$$\langle\beta\rangle = (\beta^2_x + \beta^2_y + \beta^2_z)^{1/2}, \quad (1)$$

Where

$$\beta_x = \beta_{xxx} + \beta_{xyy} + \beta_{xzz},$$
$$\beta_y = \beta_{yyy} + \beta_{xxy} + \beta_{yzz},$$
$$\beta_z = \beta_{zzz} + \beta_{xxz} + \beta_{yyz}. \quad (2)$$

HOMO and LUMO energy values,

electronegativity, and chemical hardness can be calculated as follows: $\chi = (I + A)/2$ (electronegativity), $\eta = (I - A)/2$ (chemical hardness), $S = 1/2\eta$ (global softness), $\omega = \mu^2/2\eta$ (electrophilicity) where I and A are ionization potential and electron affinity, and $I = -E_{HOMO}$ and $A = -E_{LUMO}$, respectively [38, 39]. The electronic transition properties which include the maximum excitation wavelength (λ_{max}) and relative intensities (oscillator strengths, f), were obtained by the time dependant density functional theory (TD-DFT), [40] using "A new hybrid exchange-correlation functional using the Coulomb-attenuating method (CAM-B3LYP)," at the 6-311G (d, p) bases set [41]. The population analysis has also been performed by the natural bond orbital method [42] at B3LYP/6-311G (d, p) level of theory using natural bond orbital (NBO) under Gaussian 09 program package. The second-order Fock matrix was used to evaluate the donor-acceptor interactions in the NBO basis [43]. For each donor (i) and acceptor (j), the stabilization energy $E^{(2)}$ associated with the delocalization $i \rightarrow j$ is estimated as

$$E^{(2)} = \Delta E_{ij} = q_i (F(ij)^2 / \varepsilon_j - \varepsilon_i), \quad (3)$$

Where q_i is the donor orbital occupancy, ε_i and ε_j are diagonal elements and (ij) is the off-diagonal NBO Fock matrix element. For the conversion factors of α, β, and HOMO and LUMO energies in atomic and cgs units: 1 atomic unit (a.u.) = 0.1482×10^{-24} electrostatic unit (esu) for polarizability $\langle\alpha\rangle$; 1 a.u. = 8.6393×10^{-33} esu for first hyperpolarizability $\langle\beta\rangle$; 1 a.u. = 27.2116 eV for HOMO and LUMO energies.

RESULT AND DISCUSSION:

Electronic structure

Geometry structure

Fig. 1 presents the optimized structures and the vector of the dipole moment of the studied compounds **1-6** using the B3LYB/6-311G (d, p). The energies of HOMO, LUMO, energy gap and dipole moment of all compounds are presented in Fig. 2 and Table 3. The optimized geometrical parameters (bond lengths, bond angles and dihedral angles) of the studied compounds **1-6**, is listed in Tables 1 and 2. The analysis of Tables 1 and 2 and Figs. 1 and 2 shows that:

The most stable geometry of the studied compounds, **1-6**, is the planar structures as indicated from the dihedral angles (c.f. Table 2). The calculated bond lengths and bond angles for the studied compounds, **1-6** using B3LYP/6-311G (d,p) are in good agreement with the reported X-ray data [44, 45].

The optimized bond length of carbon-carbon in the benzo rings fall in the range from 1.387 to 1.509 Å in the studied compounds **1-6** (c.f. Table 1). The compound shows no extended conjugation involving the carbon-carbon bonds, since the C-C and C=C bond lengths are significantly larger and shorter, respectively, than the C-C bond lengths in a typical aromatic six-member ring (Ca. 1.39Å). Indeed, the C-C bond lengths in the studied compounds **1-6** (1.449-1.479Å) were found to be similar to the central bond in butadiene (1.463Å) [44], while the C=C bond lengths (1.387-1.390Å) do not differ very much from the C=C bond length in ethylene [45]. These conclusions are suggested by the considerably large O-C bond lengths and shorten C=O bond length (c.f. Table 1). The computed bond angles are largely affected by the presence of C=O group in C-4, especially <C8C9C10, <C3C4O11 and <O1C2H19 angles (Table 1). The optimized of the dihedral angles of the studied compounds **1-6** located near 0.0

and 180° indicating that, these compounds **1-6** are planar structure (c.f. Table 2).

Table 1: Selected experimental and theoretical bond lengths, and bond angles for the studied compounds **(1-6)** computed at the B3LYP/6-311G (d,P) level of theory

Parameters	EXP.[44,45]	1	2	3	4	5	6
Bond lengths (Å)							
O1 –C2	1.341	1.336	1.335	1.335	1.337	1.337	1.338
C2-C3	1.363	1.355	1.356	1.355	1.355	1.355	1.354
C3-C4	1.471	1.481	1.481	1.481	1.480	1.480	1.478
C4-C5	1.501	1.490	1.489	1.489	1.492	1.492	1.495
C5-C6	1.405	1.396	1.394	1.393	1.395	1.395	1.396
C6-C7	1.392	1.393	1.393	1.402	1.393	1.393	1.401
C7-C8	1.385	1.387	1.384	1.389	1.385	1.385	1.385
C8-C9	1.451	1.402	1.409	1.408	1.401	1.400	1.399
C9-C10	1.395	1.384	1.388	1.386	1.382	1.382	1.381
C10-C5		1.402	1.403	1.403	1.404	1.401	1.401
C2-H19	1.095	1.085	1.092	1.082	1.081	1.084	1.099
C3-C12	1.435	1.481	1.485	1.485	1.484	1.453	1.484
C12-O13	1.275	1.203	1.281	1.251	1.233	1.202	1.214
C12-H18	1.095	1.085	1.092	1.082	1.081	1.084	1.099
C4-O11	1.295	1.215	1.216	1.226	1.256	1.214	1.213
C10-H17	1.095	1.083	1.085	1.084	1.084	1.092	1.096
C9-H16	1.085	1.083	1.084	1.089	1.082	1.085	1.092
C8-H15	1.085	1.084	1.091	1.091	1.094	1.082	1.081
C7-H14	1.085	1.083	1.094	1.094	1.082	1.082	1.083
C14-H20	1.085	1.083	1.094	1.094	1.093	1.094	1.083
C14-H21	1.081	1.084	1.085	1.087	1.086	1.087	1.088
C14-H22	1.095	1.083	1.083	1.086	1.083	1.084	1.085
Bond Angles (°)							
<C6O1C2	119.31	118.56	118.42	118.76	118.53	118.52	118.68
<O1C2C3	123.00	126.13	126.11	125.99	126.11	126.11	126.00
<C2C3C4	119.99	119.73	119.78	119.67	119.82	119.82	119.72
<C3C4C5	115.95	113.16	113.12	113.31	113.03	113.03	113.24
<C4C5C6	115.80	121.09	121.04	121.09	121.11	121.09	120.61
<C5C6O1	120.96	121.31	121.51	121.15	121.41	121.42	121.74
<C5C6C7	121.55	122.14	121.66	122.63	121.85	121.83	120.52
<C6C7C8	118.69	118.56	118.66	116.63	118.98	118.96	119.70
<C7C8C9	120.41	120.55	121.60	122.87	119.67	119.70	119.45
<C8C9C10	119.41	120.03	118.18	118.29	121.21	121.22	121.35
<C9C10C5	120.99	120.57	121.62	121.06	119.62	119.61	119.39
<O1C2H19	117.61	111.08	118.28	118.52	118.67	111.05	119.60
<C3C12O13	125.00	126.66	111.14	111.19	111.06	122.83	110.88
<C3C12H18	122.99	112.68	122.74	120.58	122.83	116.16	112.80
<C3C4O11	125.92	124.76	124.74	124.58	116.20	126.51	125.12
<O11C4C5	125.00	122.07	122.13	122.10	126.51	112.73	121.64
<C5C10H17	117.95	117.47	117.03	120.38	112.74	125.04	119.79
<H17C10C9	120.36	121.96	121.35	117.28	125.00	121.93	118.34
<C10C9H16	119.96	120.11	121.51	121.65	121.96	121.96	122.28
<C9C14H22	110.35	111.35	111.25	110.25	111.99	110.25	112.25
<C9C14H21	111.43	111.43	111.13	110.16	112.39	113.16	115.16
<C9C14H20	112.68	111.68	111.13	111.91	110.80	111.91	111.00
<C9C8H16	118.29	119.29	119.37	118.21	118.98	119.21	119.72
<H16C8C7	119.98	119.98	119.03	119.48	120.19	121.48	123.24

Table 2: Dihedral Angles (^{0}) and Natural Charge for the studied compounds **(1-6)** computed at the B3LYP/6-311G (d,P) level of theory

Parameters	1	2	3	4	5	6
Dihedral Angles (^{0})						
C6O1C2C3	-0.01325	0.00640	0.0000	-0.00536	0.00572	0.0061
O1C2C3C4	-0.01960	0.00997	0.0000	0.01092	0.01590	0.01141
C2C3C4C5	0.04246	-0.01898	-0.00038	-0.01059	-0.03206	-0.01053
C3C4C5C6	-0.01781	0.01380	0.00069	0.00445	0.03044	0.00404
C4C5C6O1	0.00816	0.00112	-0.00063	0.00226	-0.01184	0.00244
C5C6C7C8	-0.00210	-0.01192	0.00030	-0.00040	-0.00766	-0.00143
C6C7C8C9	0.00137	-0.00810	0.00000	0.00000	0.00116	-0.00053
O1C2C3H19	179.99646	-0.00567	0.0000	0.00000	0.00000	179.9977
C3C12O13H18	179.98623	0.01904	0.0000	0.00000	0.00000	179.99695
C2C3C12H18	0.03504	-0.01922	-0.00038	-0.00028	179.9977	179.9977
C2C3C12O13	179.95212	0.00619	0.00069	0.00053	179.99695	179.99695
C2C3C4O11	179.96106	0.00790	-0.00063	179.9977	179.9977	179.9977
C3C4O11C5	179.99618	179.9899	0.00030	179.99695	179.99695	179.99695
C12C3C4O11	0.04227	179.9964	0.00000	-0.00135	179.9977	179.9977
O11C4C5C10	-0.02619	0.00818	0.0000	-179.9976	179.99695	179.99695
C4C5C10H17	-0.00340	179.9785	0.0000	-0.00390	179.9977	0.00000
C5C10H17C9	179.99741	-0.01766	-0.00038	179.9979	179.99695	179.998
H17C10C9H16	-0.00487	179.9925	0.00069	0.00418	179.9977	-0.00079
C10C9H16C8	180.0000	-0.00958	0.00030	-0.00051	0.00054	0.00000
H16C9C8H15	0.00168	-0.00135	0.00050	-179.9992	0.000025	179.998
C9C8H15C7	179.99907	179.9991	0.00070	179.9989	0.000036	-0.00079
H15C8C7H14	0.00000	0.00020	0.00020	179.9989	179.99695	0.00000
Natural Charge						
C9	0.51359	0.51389	0.51417	0.51463	0.51445	0.51557
C12	-0.28723	-0.58379	-0.58324	-0.28583	-0.28599	-0.28337
O15	-0.53514	-0.53792	-0.53899	-0.52938	-0.52929	-0.52457
O16	-0.46211	-0.46126	-0.46800	-0.45999	-0.45979	-0.45262
O17	-0.48358	-0.48507	-0.48536	-0.48016	-0.48012	-0.47704
Br19	--------	--------	--------	0.07416	------	------
Cl19	--------	--------	--------	---------	0.00850	0.01910
Cl18	--------	--------	--------	---------	----------	0.03631

Ground state properties

The ionization energy, I.E, of compound **1** which measures the donating property (oxidation power) is 6.73 eV (c.f. Table 3). The effect of substituent's of different strengths and hence in the donating properties follows the order: **3** > **2** > **1** > **4** > **5** > **6** as shown in Table 3 and Fig. 2. However the electron affinity, E.A., of **1** which measures the accepting property (reducing power) is 2.12 eV. The order of accepting properties of 3-fromyl-chromone derivatives compounds follows **3** < **2** < **1** < **4** < **5** < **6** as shown in Table 3 and Fig. 2. The band gap, E_{gap}, is the energy gap between E_{HOMO} and E_{LUMO}, it signifies the facile electron transition from E_{HOMO} to E_{LUMO}, i.e. the reactivity of molecules in the studied compounds **1-6** are governed by their chemical structures. The results in Table 3 and Fig. 2 shows that the computed reactivity in the gas phase of the studied compounds increases in the order: **6** > **5** > **4** > **1** > **2** > **3**. This indicates that the smaller the E_{gap}, the higher the reactivity of these compounds. Finally, the theoretically computed dipole moment, μ, for compound **1** which measures the charge separation over the molecule is 6.31 D. The general trend of

the dipole moment changes for the studied 3-fromyl-chromone derivatives follow the order **3** > **6** > **2** > **5** > **4** > **1** (c.f. Table 3) and the vector of the dipole moment is presented in Fig. 1.

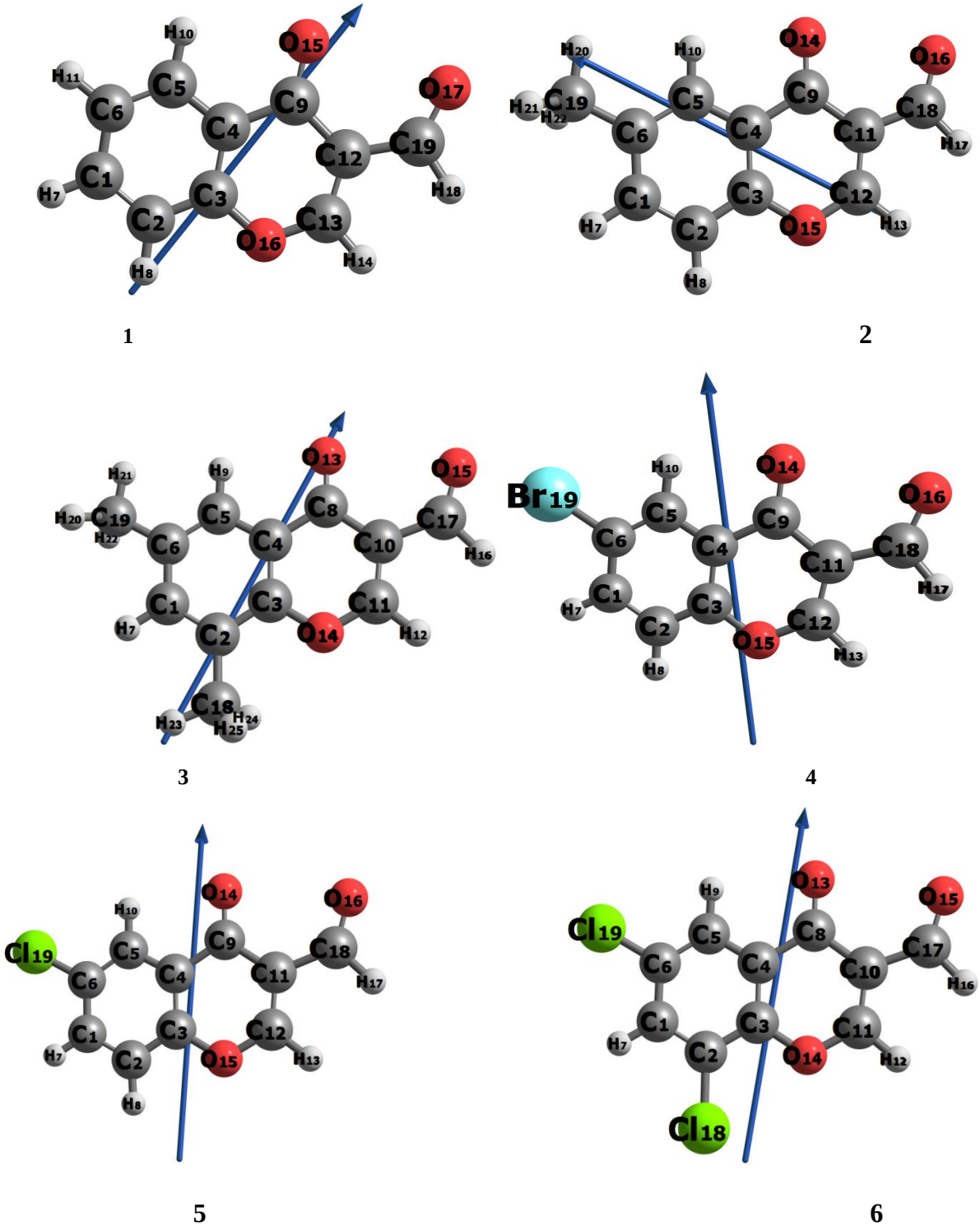

Fig. 1. The optimized structure, perspective view of dipole moment of the studied compounds **1-6** at B3LYP/6-311G (d, p).

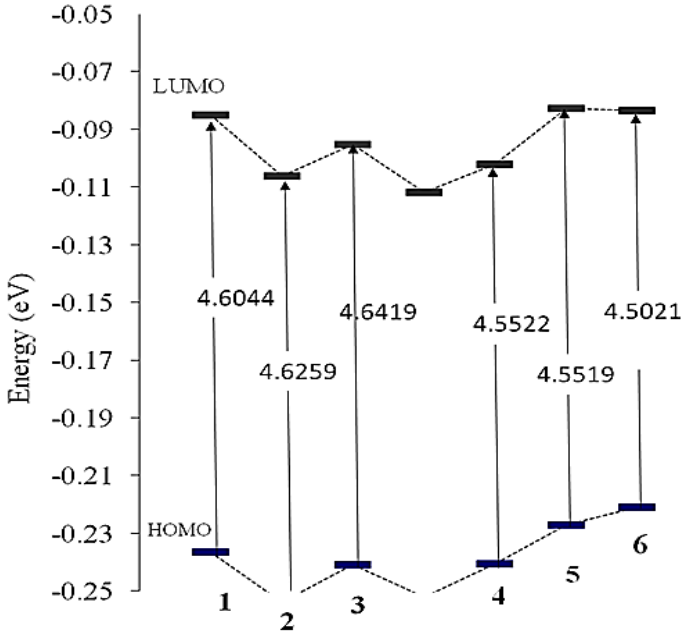

Fig. 2. Energy of HOMO, LUMO and energy gap of the studied compounds **1-6** at B3LYP/6-311G (d, p) level of theory.

1	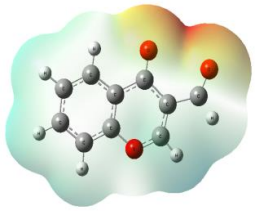	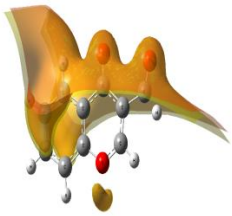	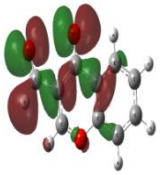	
	MEP	ESP	HOMO	LUMO
3	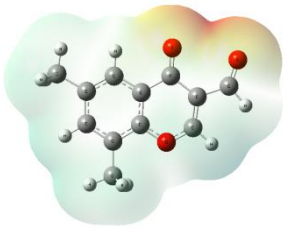	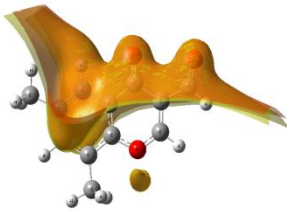	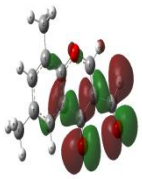	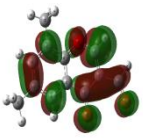
	MEP	ESP	HOMO	LUMO
4	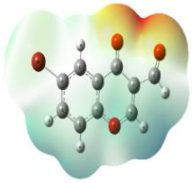	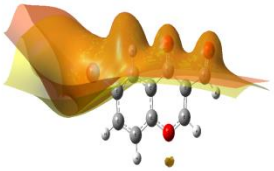	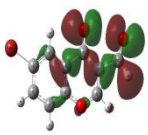	
	MEP	ESP	HOMO	LUMO

6	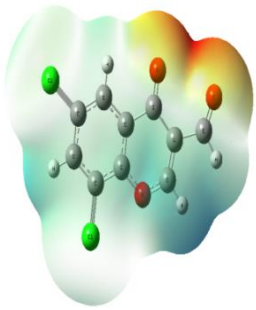	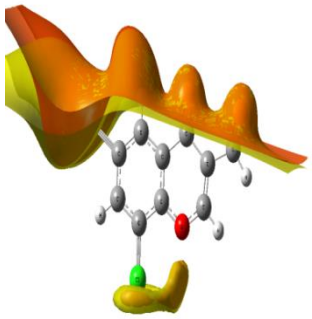	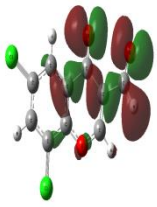	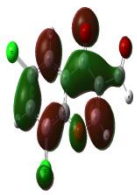
	MEP	ESP	HOMO	LUMO

Fig.3. Molecular surfaces of some studied compounds **1,3,4,6** at B3LYP/6-311G (d, p).

Table 3: Total energy, energy of HOMO and LUMO, energy gap , dipole moment, The ionization potential (**I** /eV), electron affinity (**A** /eV), chemical hardness (***η*** / eV), global softness (**S**/eV^{-1}), chemical potential (***V***/eV^{-1}), electronegativity (***χ***/eV), and global electrophilicity index, (***ω***/eV), of the studied compounds (**1-6**) computed at the B3LYP/6-311G (d,P)

Compounds	**1**	**2**	**3**	**4**	**5**	**6**
E_T (au)	-610.4794	-649.8075	-689.1360	-3184.0191	-1070.0985	-1529.7132
E_{HOMO} (eV)	-6.72792	-6.66264	-6.61912	-6.90826	-6.91914	-7.07608
E_{LUMO} (eV)	-2.12350	-2.03674	-1.97717	-2.35606	-2.36722	-2.57339
E_{gap} (eV)	4.60442	4.62590	4.64195	4.55219	4.55190	4.50214
μ (Debye)	6.31200	6.45980	6.86940	6.36100	6.42980	6.82990
I *(eV)*	6.72792	6.66264	6.61912	6.90826	6.91914	7.07608
A*(eV)*	2.12350	2.03674	1.97717	2.35606	2.36722	2.57339
X*(eV)*	4.42571	4.34969	4.29814	4.63216	4.64318	4.82474
V*(eV^{-1})*	-4.42571	-4.34969	-4.29814	-4.63216	-4.64318	-4.82474
η*(eV)*	2.30221	2.31295	2.32098	2.27610	2.27596	2.25107
S*(eV^{-1})*	0.21718	0.21617	0.21543	0.21967	0.21969	0.22212
ω (eV)	4.25394	4.08997	3.97979	4.71353	4.73629	5.17046

Global reactivity descriptors

They include HOMO, LUMO, energy gap (E_g), chemical hardness (η), electronegativity (X), chemical potential (V), electrophilicity (ω), electron affinity (A), ionization potential (I) and global softness (S) which are calculated at B3LYP/6-311G (d,p). The frontier molecular orbital (FMO) energies were calculated for the studied compounds at the same level of theory. The electron donating ability characterized by HOMO energy, while LUMO energy characterizes the electron withdrawing ability. The molecular chemical stability characterizes by Energy gap (E_g) between HOMO and LUMO which is a critical parameter in determining molecular electrical transport properties because it is a measure of electron conductivity. The results in Figs. 2, 3 and Table 3 indicate that the smaller the energy

gap the easier the charge transfer and the polarization occurs within the molecule. Furthermore, the order of increasing reactivity in the studied compounds is: **6 > 5 > 4 > 1 > 2 > 3.** The insignificant differences in E_g of all the studied compounds except **6** is due to the non-planarity of the two ph-X and ph-Y with the 3-fromyl-chromone (c.f. Table 3). Using HOMO and LUMO energies, ionization potential and electron affinity can be expressed as I~ $-E_{HOMO}$, A~ $-E_{LUMO}$ at the B3LYP/6-311G (d,p) as shown in Table 3. The variation of electronegativity (*X*) values is supported by electrostatic potential, for any two molecules, where electron will be partially transferred from one of low *X* to that of high *X*. The results show that the order of decreasing *X* is: **6 > 5 > 4 > 1 > 2 > 3**. The results of small η values for the studied compounds reflect the ability of charge transfer inside the molecule. Therefore, the order is: **6 > 5 > 4 > 1 > 2 > 3**. There is a linear relationship between η and E_g as shown in Table 3. Considering η values, the higher the η values, the harder is the molecule and vice versa.

Natural Charge

The natural population analysis [46] performed on the electronic structures of compounds **1-6** clearly describes the distribution of electrons in various sub-shells of their atomic orbits. The accumulation of charges on the individual atom presented in Table 2. In case of our studied compounds **1-6**, the most negative centers are C12, O15, O16, O17, Br19, Cl18, and Cl19-atoms. According to an electrostatic point of view of the molecule, these negative atoms have a tendency to donate an electron. Whereas, the most electropositive atoms such as; C9 have a tendency to accept an electron.

Nonlinear optical (NLO) Analysis

No experimental or theoretical investigations were found addressing NLO for these classes of molecules; therefore, this triggered our interest to undertake this study. NLO is at the forefront of current research due to its importance in providing key functions of frequency shifting, optical modulation, switching , laser, fiber, optical materials logic and optical memory for the emerging technologies in areas such as telecommunications, signal processing and optical inter connections [47]. In order to investigate the relationship between molecular structure and NLO, the polarizibilities and hyperpolarizibilities of the studied compounds **1-6** are calculated using DFT/B3LYP/6-311G (d,p). Total static dipole moment (μ), the mean polarizibility α, the anisotropy of the polarizability Δα, the mean first-order hyperpolarizibility (β) of the studied compounds **1-6** are listed in Table 4. P-nitro aniline (PNA) is a standard prototype used in NLO studies. In this study, PNA is chosen as a reference as there were no experimental values of NLO properties of the studied compounds. The values of α, β in Table 4 show that the order of increasing α with respect to PNA is : compounds **5**, **4** and **6** are ~ 2, 2.5 and 3 times higher than (PNA), whereas compounds **1, 2** and **3** are ~ 1.5 times higher than the standard (PNA) respectively, The calculated first order hyperpolarizability of p- nitroacetanilide (PNA) is 15.5×10^{-30} esu as reported by T. Gnanasambandan et al [48-50]. The analysis of the β parameter show that compounds **5, 4** and **6** are ~ 2.5, 3 and 4 times higher than (PNA), while compounds **1, 2** and **3** are ~ 1.5, 2 and 2.5 times higher than the reference

respectively. Therefore, the studies compounds show promising optical properties.

Table 4: Total static dipol moment (**μ**), the mean polarizability (<**α**>), the anisotropy of the polarizability (**Δα**), and the mean first-order hyperpolarizability (<**β**>), for the studied compounds (**1-6**) computed at B3LYP/6-311G (d,P)

Property	PNA	**1**	**2**	**3**	**4**	**5**	**6**
μ_x, D		4.5920	-4.2654	4.9680	1.0279	-1.4892	1.9752
μ_y, D		4.3307	4.8513	4.7442	6.2774	6.2550	4.4075
μ_z, D		-0.0001	0.0002	0.0000	-0.0006	-0.0007	0.0000
μ, Debye [a]	2.44	6.312006	6.459779	6.869411	6.361001	6.429832	4.829911
α_{XX}, a.u.		-74.7770	-77.8929	-90.713	-94.3049	-91.2207	-107.0126
α_{XY}, a.u.		-12.5170	14.4965	-15.385	-15.9768	11.3729	-15.8745
α_{YY}, a.u.		-72.0311	-81.7618	-85.3706	-94.1978	-87.8364	-104.1678
α_{ZZ}, a.u.		-74.6315	-80.9247	-87.2293	-92.1924	-86.4861	-98.3032
α_{YZ}, a.u.		-0.0031	0.0001	-0.0001	0.0014	0.0020	0.0005
α_{XZ}, a.u.		0.0081	-0.0051	-0.0001	0.0015	-0.0012	-0.0013
$<\alpha> \times 10^{-24}$ esu [b]	22	32.94	35.88	38.64	48.86	45.11	58.74
$\Delta\alpha \times 10^{-24}$ esu		42.37	47.58	45.27	51.12	50.85	55.55
βxxx,a.u.		75.4356	-62.6940	80.8711	110.5981	-17.5968	65.6833
βxxy,a.u.		30.9137	45.0591	46.3739	68.7695	66.7493	72.4733
βxyy,a.u.		7.5115	-15.1275	14.3252	65.9684	-24.0628	8.6887
βyyy,a.u.		13.1164	17.7208	15.6558	11.8139	21.6739	16.0613
βxxz,a.u.		-0.0197	-0.0109	0.0000	-0.0040	0.0019	0.0083
βxyz,a.u.		-0.0023	0.0009	-0.0001	-0.0052	-0.0004	0.0007
βyyz,a.u.		0.0091	0.0065	-0.0002	-0.0023	0.0010	-0.0013
βxzz, a.u.		-14.0269	11.4435	-11.6649	23.6736	9.0058	-8.0686
βyzz, a.u.		-0.9323	-3.6214	-0.5358	-12.0870	-5.4940	-1.3280
βzzz, a.u.		-0.0034	-0.0009	0.0001	0.0021	0.0010	-0.0003
$<\beta> \times 10^{-30}$ esu [c]	15.5	26.15	33.28	38.12	46.09	44.12	58.40

a, b, c PNA results are taken from references [48-50].

Molecular electrostatic potential (MEP)

The electronic density is related by Molecular electrostatic potential (MEP) and is a very useful descriptor in understanding sites for electrophilic and nucleophilic attack as well as hydrogen bonding interactions [51]. This is correlated with dipole moments, electro negativity, partial charges and chemical reactivity of the molecules. These maps allow us to visualize variably charged regions of a molecule. Knowledge of the charge distributions can be used to determine how molecules interact with one another. The calculated 3D MEP and ESP of some of the studied molecules (**1,3,4,6**) are calculated from optimized molecular structure using DFT/B3LYP/6-311G (d,p) are shown in Figs. 3 and 4. The results show that , in case of **1** (X=Y=H) the

negative region (red) is mainly over the O atomic sites, which is caused by the contribution of lone-pair electron of oxygen atom while the positive (blue) potential sites are around the hydrogen, and carbon atoms. A portion of the molecule that has negative electrostatic potential will be susceptible to electrophilic attack—the more negative the higher the tendency for electrophilic attack. The color scheme for the MEP surface is as follows: red for electron rich, (partially negative charge); blue for electron deficient, (partially positive charge); light blue for (slightly electron deficient region); yellow for (slightly electron rich region); green for neutral (zero potential) respectively. Potential increases in the following order: red < orange < yellow < green < blue [52,53].

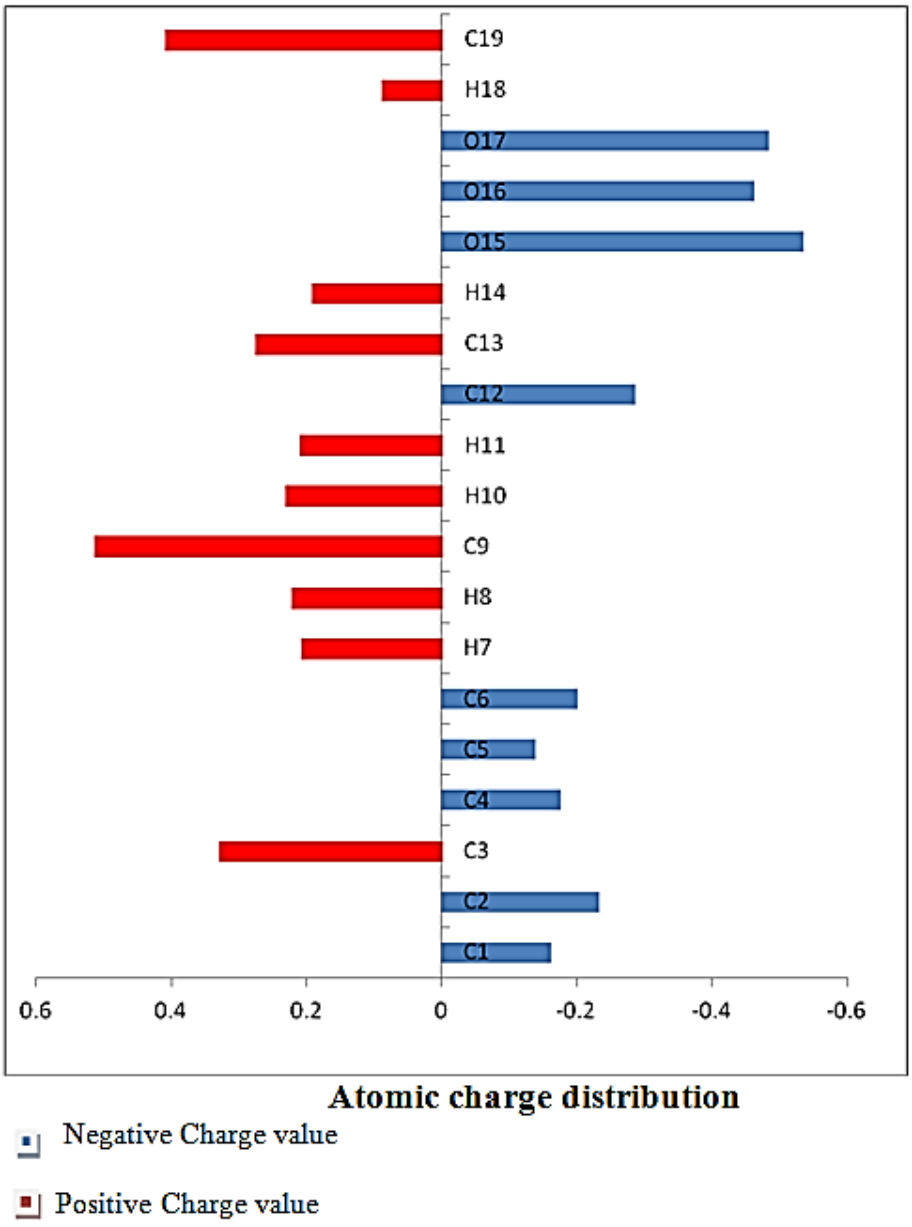

Fig. 4. Atomic charge distribution (au) for chromone-3-carboxaldehyde **1** at B3LYP/6-311G (d,p) basis set.

Electronic absorption spectra of compound 1

Fig. 5 and Table 6 presents the experimental and theoretical electronic absorption spectra of **1** in dioxane and ethanol. The spectrum of **1** is composed of five bands in the range 200–400 nm. The spectrum in dioxane shows three intense bands at 250 nm, 228 nm, and 210 nm. Increasing solvent polarity on going from dioxane to ethanol results in a blue shift with the first band is shifted to 245 nm, the second band is shifted to 224 nm, and the third band is shifted to 206 nm, respectively. The three observed bands are assigned as (π–π*) transitions, as indicated by the values of molar absorptive (ε =45000). In order to account for the experimentally observed UV Spectra of **1** in dioxane and ethanol, it is essential to consider the theoretically calculated vertical transitions using TD-DFT-CAM-B3LYP/6-311G (d, p) level. The experimental band at 250 nm (in dioxane) is reproduced theoretically by using PCM (dioxane), at 243 (state I) nm, and in gas phase at 241 nm as shown in Table 6. The theoretical calculations of single point energy vertical excitations in ethanol reproduce the wavelength of this band at 243 nm (state I), indicating that the calculated wavelength is lower than the observed wavelength. The second band observed experimentally at 228 nm in dioxane, is reproduced theoretically at 222 nm (state II). The gas phase calculation gives a wavelength at 218 nm. Moreover, In ethanol, this same band appears at 224 nm, where theoretical calculations in ethanol reproduce this band at 222 nm (state II), as shown in Table 6. The third $(\pi\text{-}\pi^*)^1$ state observed experimentally at 210 nm in dioxane, is reproduced theoretically at 203 nm (state III), which involves the orbital's φ_{43} and $\varphi_{47,}$ in the transition. The gas phase calculation gives a wavelength at 201 nm (state III), which also involves orbital's φ_{41} and φ_{46}. In ethanol, this same band appears experimentally at 206 nm, is reproduced theoretically at 201 nm, (state III), as shown in Table 6. The fourth and five $(\pi\text{-}\pi^*)^1$ state theoretically at 187 and 176 nm in dioxane, respectively, (state IV and V), which involves the orbital's φ_{41} and $\varphi_{46,}$ φ_{43} and φ_{48} in the transition. The gas phase calculation gives a wavelength at 185 and 174 nm respectively, (state IV and V), in ethanol, this same band appears theoretically at 186 and 176 nm respectively, (state IV and V), as shown in Table 6. The nature of the electronic transition can be inferred from examining the electron density contours of molecular orbitals. The six orbital's φ_{43} - φ_{48}, involved in the theoretical transitions of **1**, are shown in Fig. 11, show a delocalization of electron density, and Charge Transfer CT character.

The NBO analysis of the studied compounds **1-6** provides an efficient method for studying intra-and intermolecular bonding and also provides a convenient basis for investigating charge transfer or conjugative interactions in molecular systems. Table 5 presents the second order perturbation energies of most interacting NBOs of **1-6** and the most important interaction between filled (donor) Lewis type NBOs and empty (acceptor) non-Lewis NBOs. The charge density maps of HOMO and LUMO for **1-6** are presented in Fig.11. The results of NBO analysis of compound **1** tabulated in Table 5 indicate that there is a strong hyper conjugative interactions $\pi^*C_1\text{-}C_2 \rightarrow \pi^*C_5\text{-}C_6$, $\pi^*C_3\text{-}C_4 \rightarrow \pi^*C_9\text{-}O_{15}$, LP (2) $O_{16} \rightarrow \pi^*C_{12}\text{-}C_{13}$, LP (2) $O_{17} \rightarrow \sigma^*H_{18}\text{-}C_{19}$, and $\pi C_1\text{-}C_2 \rightarrow \pi^*C_3\text{-}C_4$, for **1** is 214.94, 150.61, 34.85, 24.47, and 22.42 kcal/mol, respectively. The C–O π orbital in aldehyde group and quinoline ring interacts equally well with chromone ring. In fact, its interaction with the chromone

ring is greater. Furthermore, the lone pair orbital of the oxygen atom enjoys hyperconjugation with the C9–O15, and C1–C2 π* orbital. It is surprising to notice a decrease in the population of the NBO C1–C2, and C3–C4 reflecting a charge transfer away from the 3-fromyl-chromone ring. In conclusion, **1** enjoys the linear conjugation that is responsible for the observed spectrum. No specific part of the molecule manifests itself in the observed spectrum.

Table 5. Second Order Perturbation Interaction Energy Values Computed in the NBO Basis for the studied compounds **1-6**, calculated at B3LYP/6-311G (d, p)

Compound	Donor	Acceptor	$E^{(2)a}$(kcal/mol)	NBO	Population
1H	πC1-C2	π*C3- C4	22.42	πC1-C2	1.68530
	πC12-C13	π*C9-O15	20.10	C12-C13	1.79601
	LP (1) O15	RY*C9	13.42	LP (1) O15	1.97868
	LP (2) O15	σ*C9-C12	21.32	LP (2) O15	1.87761
	LP (2) O16	π*C12-C13	34.85	LP (2) O16	1.73139
	LP (1) O17	RY*C19	12.25	LP (1) O17	1.98334
	LP (2) O17	σ*H18-C19	24.47	LP (2) O17	1.86799
	π*C1- C2	π*C5-C6	214.94	π*C1- C2	0.30273
	π*C3-C4	π*C9- O15	150.61	π*C3-C4	0.41072
2CH3	πC1-C2	π*C3- C4	21.43	πC1-C2	1.69728
	LP (2) O15	π*C11-C12	35.15	LP (2) O15	1.73065
	π*C1- C2	π*C5-C6	139.99	π*C1- C2	0.29482
	π*C3-C4	π*C9- O14	180.51	π*C3-C4	0.41081
3di-CH3	πC1-C2	π*C3- C4	21.03	πC1-C2	1.68164
	LP (2) O14	π*C3- C4	23.91	LP (2) O14	1.73198
	π*C3- C4	π*C1-C2	242.27	π*C3- C4	0.40876
	π*C10-C11	π*C8- O13	61.35	π*C3-C4	0.20272
4Br	πC1-C2	π*C3- C4	21.69	πC1-C2	1.69728
	πC6- Br19	π*C4-C5	3.36	πC6- Br19	1.98179
	LP(3) Br19	σ*C5-C6	10.01	LP(3) Br19	1.93327
	π*C3-C4	π*C9- O14	128.89	π*C3-C4	0.40940
5Cl	LP (2) O15	π*C3- C4	25.03	LP (2) O15	1.73180
	LP (3) Cl19	σ*C5-C6	13.43	LP (3) Cl19	1.93371
	πC6-Cl19	π*C4-C5	5.32	πC6-Cl19	1.98769
	π*C3-C4	π*C9- O14	127.73	π*C3-C4	0.41002
6di-Cl	πC1-C2	π*C3- C4	19.99	πC1-C2	1.70321
	LP (2) O14	π*C10- C11	33.71	LP (2) O14	1.73141
	LP (3) Cl18	π*C1-C2	13.43	LP (3) Cl18	1.91967
	LP (3) Cl19	σ*C5- C6	12.96	LP (3) Cl19	1.92191
	π*C3-C4	π*C8- O13	103.62	π*C3-C4	0.41159
	πC2-Cl18	π*C3-C4	26.43	πC2-Cl18	1.97869
	πC6-Cl19	π*C4-C5	25.33	πC6-Cl19	1.98659

[a] $E^{(2)}$ means energy of hyperconjugative interactions (stabilization energy).
$LP_{(n)}$ is a valence lone pair orbital (n) on atom.

Table 6. Theoretical and experimental UV spectra of **1**, calculated at CAM-B3LYP/6–311G (d, p)

	TD-Theoretical												Experimental	
	Gas phase				Dioxane				Ethanol				Dioxane	Ethanol
state	Configuration	Coefficient	f	λ, nm	Configuration	Coefficient	f	λ, nm	Configuration	Coefficient	f	λ, nm	$\lambda_{,nm}$	$\lambda_{,nm}$
I	41->46 43->46 43->47 44->46 44->47	-0.15 0.18 -0.12 0.29 0.57	0.111	241	41->46 43->46 43->47 44->46 44->47	-0.15 0.17 -0.11 0.29 0.57	0.161	243	41->46 43->46 43->47 45->46 45->47	0.14 -0.21 -0.13 -0.28 0.56	0.131	243	250	245
II	43->46 43->47 44->47	0.64 -0.12 -0.21	0.284	218	43->46 43->47 44->47	0.64 -0.17 -0.20	0.423	222	41->47 43->46 43->47 45->47	-0.11 0.64 0.10 0.24	0.482	222	228	224
III	41->46 41->47 43->46 43->47 44->46 44->47 44->48	0.43 -0.25 0.17 0.38 0.12 0.11 0.17	0.269	201	41->46 41->47 43->47 43->48 44->46 44->47 44->48 44->49	-0.25 0.33 0.42 -0.16 0.23 -0.13 0.13 0.17	0.119	203	41->46 41->47 43->46 43->47 45->46	-0.40 -0.24 -0.16 0.45 -0.13	0.302	201	210	206
IV	41->46 43->47 43->48 44->48	0.14- -0.21 0.12 0.62	0.272	185	41->46 41->47 43->46 43->47 44->46	0.41 -0.28 0.19 0.40 0.11	0.349	187	43->47 43->49 45->48	0.17 0.10 0.66	0.251	186		
V	41->47 43->48 44->46 44->47	0.35 0.54 -0.10 0.16	0.321	174	41->47 43->47 43->48 44->47	0.33 0.11 0.56 0.16	0.421	176	41->47 43->48 45->47 45->49	0.35 0.54 -0.17 0.12-	0.351	176		

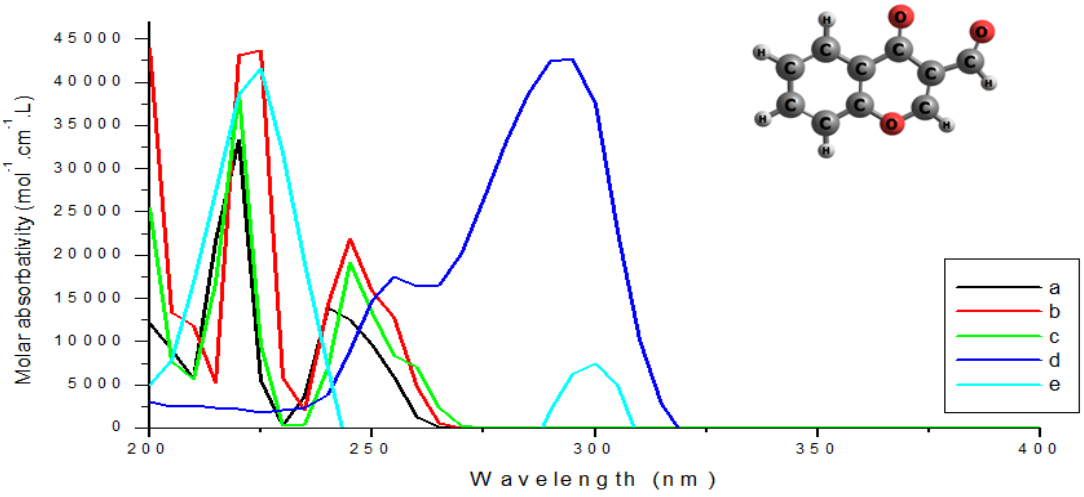

Fig. 5. Electronic absorption spectra of **1**, (a) theoretical in gas phase, (b) theoretical in dioxane, (c) theoretical in, ethanol (d) experimental in dioxane, (e) experimental in ethanol.

Electronic absorption spectra of compound 2

Insertion of CH3 group in position X in Ph-X of compound **1** gives compound **2.** The experimental and theoretical electronic absorption spectra of compound **2** in dioxane and ethanol are shown in Fig. 6 and Table 7. In dioxane, the experimental spectrum is composed of three bands, at 255 nm, 229 nm, and 207 nm. Increasing solvent polarity from dioxane to ethanol results in a blue shift of the three bands, where the first band is shifted to 250 nm, the second band is shifted to 226 nm, and the third band is shifted to 204 nm, respectively. Furthermore, increasing solvent polarity causes a marked increase in the intensity of both bands. The three observed bands are assigned as (π–π*) transitions, based on the values of molar absorptive (ε = 320000). The interpretation of the experimentally observed UV Spectra of **2** in dioxane and ethanol requires the theoretical calculations of the vertical transitions using CAM / B3LYP/6-311G (d, p) level. In dioxane, the band appearing in the experimental spectrum at 255 nm is reproduced theoretically using dioxane as a solvent at 248 nm (state I), as shown in Table 7, which involves orbital's φ_{49} and φ_{51}, showing a good agreement between the observed wavelength with the calculated wavelength. Theoretical gas phase calculations of compound **2** give a vertical excitation at 246 nm (state I), which is about 9 nm lower than the experimental wavelength, where the transition in the gas phase also involves the same orbitals. Increasing solvent polarity results in a blue shift of λ_{max} of this band to 250 nm. The theoretical calculations of the vertical excitation in ethanol reproduce the wavelength of this band at 248 nm (state I), indicating that the same orbital's are involved in this transition. It is also clear that the calculated wave length is lower than the observed wavelength. The second band observed experimentally in dioxane at 229 nm, is reproduced theoretically at 223 nm (state II), indicating that the orbital's φ_{47} and φ_{50} are involved in this transition. Theoretical gas phase calculations give a wavelength at 220 nm (state II). This same band is observed at 226 nm in ethanol, where theoretical calculations in ethanol reproduces this band at 224 nm (state II), which is lower than the observed wavelength, where the orbital's φ_{47} and φ_{50} are involved in this transition. The third $(\pi\text{-}\pi^*)^1$ state observed experimentally at 207 nm in dioxane, is reproduced theoretically at 201 nm (state III), which involves the orbital's φ_{45} and $\varphi_{50,}$ in the transition. The gas phase calculation gives a wavelength at 200 nm (state III). In ethanol, this same band appears experimentally at 204 nm, is reproduced theoretically at 202 nm, (state III), as shown in Table 7. The fourth, five, six and seven $(\pi\text{-}\pi^*)^1$ state theoretically at 196, 188, 177, and 170 nm in dioxane, respectively, (state IV, V, VI, and VII). The gas phase calculation gives a wavelength at 194, 187, 175, and 171 nm respectively, in ethanol, this same band appears theoretically at 196, 189, 177, and 170 nm respectively, as shown in Table 7. The nature of the electronic transition can be inferred from examining the electron density contours of molecular orbitals. The nine orbital's $\varphi_{45} - \varphi_{52,}$ and φ_{62}, involved in the theoretical transitions of **2**, are shown in Fig. 11, show a localization and delocalization of electron density, and Charge Transfer CT character.

The results of NBO analysis of compound **2** tabulated in Table 5 indicate that there is a strong hyper conjugative interactions $\pi^*C_3\text{-}C_4 \rightarrow \pi^*C_9\text{-}O_{14,}$ $\pi^*C_1\text{-}C_2 \rightarrow \pi^*C_5\text{-}C_6$, LP (2) $O_{15} \rightarrow \pi^*C_{11}\text{-}C_{12}$ and $\pi C_1\text{-}C_2 \rightarrow \pi^*C_3\text{-}C_4$, for **2** is 180.51, 139.99, 35.15, and 21.43 kcal/mol, respectively. NBO analysis of the p-CH3 derivative Table 5 indicates that it retained

the extended conjugation of **1** as revealed by the interaction of C–O NBOs with those of chromone ring. Furthermore, the interaction of the oxygen lone orbital's with the C9–O14, and C1–C2 π^* orbital is marked. The population of the NBO C1–C2, and C3–C4 reflecting a charge transfer away from the 3-fromyl-chromone ring. This is also evident in the case of the population of the oxygen lone orbital LP (2) O_{15}.

Table 7. Theoretical and experimental UV spectra of **2**, calculated at CAM -B3LYP/6–311G (d, p)

	TD-Theoretical												Experimental	
	Gas phase				Dioxane				Ethanol				Dioxane	Ethanol
state	Configuration	Coefficient	f	λ, nm	Configuration	Coefficient	f	λ, nm	Configuration	Coefficient	f	λ, nm	λ,nm	λ,nm
I	45->50 47->50 47->51 49->50 49->51	-0.14 0.17 -0.11 0.29 0.57	0.141	246	45 >50 47->50 49->50 49->51	0.15- 0.15 0.29 0.58	0.202	248	46->50 47->50 49->50 49->51	-0.13 0.20 0.26 0.58	0.173	248	255	250
II	47->50 47->51 49->51 49->52	0.65 -0.13 -0.17 -0.11	0.291	220	47->50 47->51 49->51	0.64 -0.19 -0.15	0.442	223	47->50 47->51 49->51	0.64 -0.13 -0.19	0.493	224	229	226
III	45->50 45->51 47->50 47->51 49->50 49->52	0.47 -0.21 0.15 0.36 0.13 0.20	0.181	200	45->50 45->51 47->50 47->51 49->50 49->52	0.42 -0.26 0.18 0.41 0.12 0.11	0.262	201	46->50 46->51 47->50 47->51 49->50 49->52	0.40 -0.22 0.15 0.47 0.12 0.11	0.243	202	207	204
IV	45->50 45->51 47->51 47->52 49->53	0.39 0.41 -0.27 0.20- 0.14	0.141	194	45->50 45->51 47->51 47->52 49->51 49->53	0.45 0.40 -0.19 -0.18 0.12 0.13	0.162	196	46->62 46->51 47->51 47->52 49->51 49->53	0.45 0.40 -0.20 0.19- 0.13 0.13	0.163	196		
V	45->50 45->51 47->51 49->52	-0.12 -0.13 -0.26 0.60	0.401	187	45->51 47->51 49->52	-0.12 -0.22 0.64	0.392	188	45->51 47->51 49->52	-0.14 -0.21 0.63	0.373	189		
VI	45->51 47->52 49->51 49->53	0.30 0.53 0.17 0.23-	0.231	175	45->51 47->52 47->53 49->51 49->53	0.28 0.56 0.10 0.17 -0.18	0.312	177	46->51 47->52 47->53 49->51 49->53	0.30 0.51 0.10 0.18 -0.27	0.223	177		
VII	45->51 47->52 49->53	-0.15 0.52 0.27	0.121	171	45->51 45->53 49->53 47->52	-0.13 0.15- 0.25 0.60	0.112	170	44->53 47->52 49->53	-0.14 0.33 0.57	0.193	170		

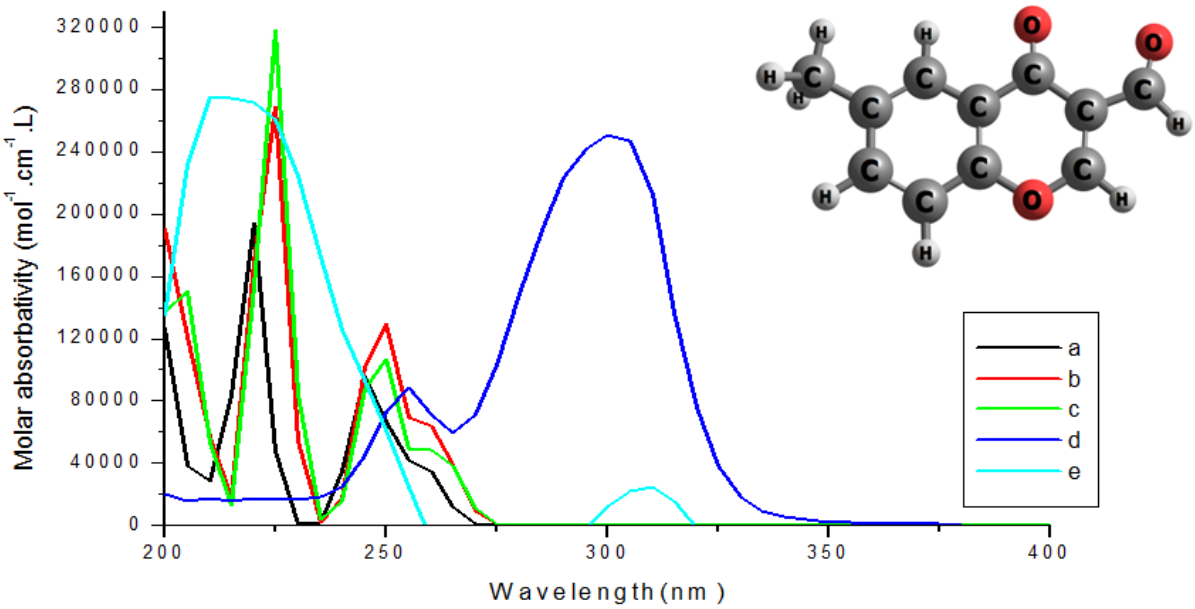

Fig. 6. Electronic absorption spectra of **2**, (a) theoretical in gas phase, (b) theoretical in dioxane, (c) theoretical in, ethanol (d) experimental in dioxane, (e) experimental in ethanol.

Electronic absorption spectra of compound 3

To complete our investigation of substituent effect on the electronic structure and spectra of compound **1**, we introduce diCH3-group in position X and Y in Ph-X-Y of compound **1** gives compound **3.** The experimental and theoretical electronic absorption spectra of compound **3** in dioxane and ethanol are shown in Fig. 7 and Table 8. The experimental spectrum in dioxane is composed of four bands at 258 nm, 234 nm, 218 nm, and 209 nm. The change of solvent polarity from dioxane to ethanol results in a blue shift of the four bands, where the first band is shifted to 255 nm, the second band is shifted to 230 nm, the third band is shifted to 215 nm, and the fourth band shifted to 206 nm, respectively. Furthermore, increasing solvent polarity causes a marked increase in the intensity of both bands. The values of molar absorptive (ε = 60000) indicates that the four observed bands have π–π* character. Theoretical transitions in the gas phase give a vertical excitation at 250 nm (state I), which is about 8 nm lower than the experimental wavelength, where it involves the same orbitals as in dioxane. Theoretical vertical excitation calculations in ethanol give λ_{max} of this band at 252 nm (state I), which shows agreement, implying that the orbitals involved in this transition are φ_{53} and φ_{55}. The experimental second band observed at 234 nm in dioxane, is reproduced theoretically at 227 nm (state II), where the calculations in dioxane indicate that the orbital's φ_{51} and φ_{54} are involved in this transition. Gas phase calculations give λ_{max} at 226 nm (state II). Theoretical calculations in ethanol show that, this band appears at 228 nm (state II), which is lower than the experimental wavelength. The third $(\pi\text{-}\pi^*)^1$ state observed experimentally at 218 nm in dioxane, is reproduced theoretically at 213 nm (state III), which involves the orbital's φ_{51} and $\varphi_{55,}$ in the transition. The gas phase calculation gives a wavelength at 212 nm

(state III). In ethanol, this same band appears experimentally at 215 nm, is reproduced theoretically at 213 nm, (state III), as shown in Table 8. The experimental fourth band observed at 209 nm in dioxane, is reproduced theoretically at 203 nm (state IV), where the calculations in dioxane indicate that the orbital's φ_{49} and φ_{55} are involved in this transition. Gas phase calculations give λ_{max} at 201 nm (state IV). Theoretical calculations in ethanol show that, this band appears at 204 nm (state IV), which is lower than the experimental wavelength. The five, six and seven $(\pi\text{-}\pi^*)^1$ state theoretically at 197, 191, and 181 nm in dioxane, respectively, (state V, VI, and VII). The gas phase calculation gives a wavelength at 195, 190, and 180 nm respectively, in ethanol, this same band appears theoretically at 197, 191, and 181 nm respectively, as shown in Table 8. The nature of the electronic transition can be inferred from examining the electron density contours of molecular orbital's. The nine orbital's $\varphi_{49} - \varphi_{57}$, involved in the theoretical transitions of **3**, are shown in Fig. 11, show a localization and delocalization of electron density, and Charge Transfer CT character.

The results of NBO analysis of compound **3** tabulated in Table 5 indicate that there is a strong hyper conjugative interactions $\pi^*C_3\text{-}C_4 \rightarrow \pi^*\ C_1\text{-}C_2$, $\pi^*C_{10}\text{-}C_{11} \rightarrow \pi^*\ C_8\text{-}O_{13}$, LP (2) $O_{14} \rightarrow \pi^*C_3\text{-}\ C_4$ and $\pi\ C_1\text{-}C_2 \rightarrow \pi^*C_3\text{-}C_4$, for **3** is 242.27, 61.35, 23.91, and 21.03 kcal/mol, respectively. NBO analysis of the diCH3 derivative Table 5 indicates that it retained the extended conjugation of **1** as revealed by the interaction of C–O NBOs with those of chromone ring. Furthermore, the interaction of the oxygen lone orbital's with the C9–C12 σ*orbital is marked. The population of the NBO C1–C2, and C3–C4, reflecting a charge transfer away from the 3-formyl-chromone ring.

Table 8: Theoretical and experimental UV spectra of **3**, calculated at CAM -B3LYP/6–311G (d, p).

	TD-Theoretical												Experimental	
	Gas phase				Dioxane				Ethanol				Dioxane	Ethanol
state	Configuration	Coefficient	f	λ, nm	Configuration	Coefficient	f	λ, nm	Configuration	Coefficient	f	λ, nm	$\lambda_{,nm}$	$\lambda_{,nm}$
I	49->54 51->54 51->55 53->54 53->55	-0.15 0.13 -0.15 0.36 0.52	0.151	250	49->54 51->54 51->55 53->54 53->55	-0.16 -0.12 0.14 0.36 0.53	0.212	252	50->54 51->54 51->55 53->54 53->55	0.15 0.16 0.15 0.34 0.53	0.173	252	258	255
II	51-> 54 51->55 53->55	0.66 -0.12 -0.17	0.261	226	51->54 51->55 53->55	0.64 -0.20 0.15	0.402	227	51->54 51->55 53->55	0.65 0.13 -0.19	0.453	228	234	230
III	49-> 54 49->55 51->54 51->55 53-> 55 53->56	0.46 -043 0.12 0.15 0.13 0.11	0.181	212	49->55 51->54 51->55 51->56 53->54 53->56 53->57	-0.22 0.16 0.55 -0.15 -0.23 -0.13 -0.14	0.122	213	50->55 51->54 51->55 51->56 53->54 53->56 53->57	-0.23 -0.12 0.56 0.16 0.23 0.12 0.15	0.103	213	218	215

IV	49- >54 49->55 51->55 51->56 51->57 53->57	0.46 0.37 -0.19 -0.23 -0.11 0.10	0.111	201	49->54 49->55 51->54 51->55 53->55 53->57	-0.44 0.46 0.13 0.15 -0.11 0.13	0.212	203	50->54 50->55 51->54 51->55 53->55 53->57	0.45 0.45 -0.12 0.17 0.10- -0.13	0.193	204	206	209
V	51->55 53->56 53->57	-0.25 0.63 0.11	0.351	195	49->54 49->55 51->55 51->56 51->57	0.50 0.36 0.17 0.18 0.10	0.162	197	50->54 50->55 51->55 51->56 51->57	0.49 -0.37 -0.19 0.18 0.11	0.153	197		
VI	49->55 51->56 53->55 53-> 57	0.29 0.54 0.21 -0.17	0.351	190	51->55 53->56 53->57	0.21 0.65 0.12	0.352	191	51->55 53->56 53->57	-0.20 0.65 0.13	0.333	191.		
VII	49->55 49->56 49->57 51->56 53->57	-0.12 0.13 -0.14 0.25 0.59	0.121	180	49->55 51->56 53->55 53->57	-0.26 0.57 -0.20 0.15	0.432	181	50->55 51->56 51->57 53->55 53->57	0.28 0.53 0.10 0.20 0.22	0.323	181		

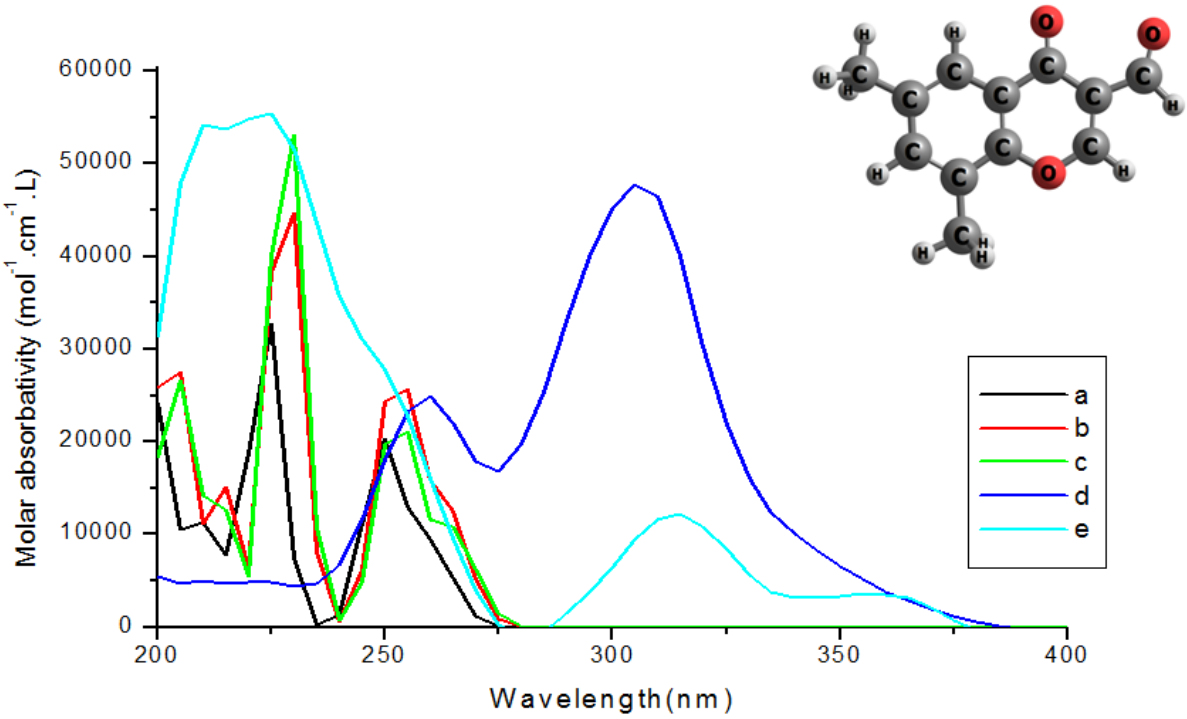

Fig. 7. Electronic absorption spectra of **3**, (a) theoretical in gas phase, (b) theoretical in dioxane, (c) theoretical in, ethanol (d) experimental in dioxane, (e) experimental in ethanol.

Electronic absorption spectra of compound 4

Compound **4** results by inserting Br-atom in position X in Ph-X of compound **1.** The experimental and theoretical electronic absorption spectra of compound **4** in dioxane and ethanol are shown in Fig. 8 and Table 9. The experimental spectrum in dioxane is composed of three bands at 250 nm, 223 nm, and 205 nm. The change

of solvent polarity from dioxane to ethanol results in a small red shift by 5 nm of the first band, the second band red shift by 3 nm, and the third band red shift by 3 nm. Additionally, increasing solvent polarity causes a marked decrease in the intensity of both bands. The values of molar absorptive (ε = 80000) indicates that the three observed bands have π–π* character. The theoretical transition of the first band in dioxane involves orbital's φ_{62} and φ_{64}, showing a good agreement between the observed and the calculated wavelengths. Theoretical transitions in the gas phase give a vertical excitation at 246 nm (state I), which is about 9 nm lower than the experimental wavelength, where it involves the same orbital's as in dioxane. Theoretical vertical excitation calculations in ethanol give λ_{max} of this band at 247 nm (state I). The experimental second band observed at 223 nm in dioxane, is reproduced theoretically at 219 nm (state II), where the calculations in dioxane indicate that the orbital's φ_{60} and φ_{63} are involved in this transition. Gas phase calculations give λ_{max} at 217 nm (state II). Theoretical calculations in ethanol show that, this band appears at 220 nm (state II), which is lower than the experimental wavelength. The third $(\pi\text{-}\pi^*)^1$ state observed experimentally at 205 nm in dioxane, is reproduced theoretically at 203 nm (state III), which involves the orbital's φ_{59} and $\varphi_{63,}$ in the transition. The gas phase calculation gives a wavelength at 201 nm (state III). In ethanol, this same band appears experimentally at 208 nm, is reproduced theoretically at 202 nm, (state III), as shown in Table 9. The fourth, five and six $(\pi\text{-}\pi^*)^1$ state theoretically at 199, 193, and 179 nm in dioxane, respectively, (state IV, V and VI). The gas phase calculation gives a wavelength at 193, 195, and 180 nm respectively, in ethanol, this same band appears theoretically at 198, 194, and 179 nm respectively, as shown in Table 9. The nature of the electronic transition can be inferred from examining the electron density contours of molecular orbital's. The eight orbital's $\varphi_{58} - \varphi_{65}$, involved in the theoretical transitions of **4**, are shown in Fig. 11, show a localization and delocalization of electron density, and Charge Transfer CT character.

The results of NBO analysis of compound **4** tabulated in Table 5 indicate that there is a strong hyper conjugative interactions $\pi^*C_3\text{-}C_4 \rightarrow \pi^*C_9\text{-}O_{14}$, $\pi\ C_1\text{-}C_2 \rightarrow \pi^*\ C_3\text{-}C_4$, and LP (3) $Br_{19} \rightarrow \sigma^*C_5\text{-}C_6$, for **4** is 128.89, 21.69, and 10.01 kcal/mol, respectively. NBO analysis of the Br derivative Table 5 indicates that it retained the extended conjugation of **1** as revealed by the interaction of C–Br NBOs with those of phenyl ring. Furthermore, the interaction of the brome lone orbital's with the C5–C6 σ*orbital is marked. The population of the NBO C1–C2, and C3–C4 reflecting a charge transfer away from the 3-fromyl-chromone ring.

Electronic absorption spectra of compound 5

Insertion of Cl-atom in position X in Ph-X of compound **1** gives compound **5.** The experimental and theoretical electronic absorption spectra of compound **5** in dioxane and ethanol are shown in Fig. 9 and Table 10. In dioxane, the experimental spectrum is composed of three bands, at 250 nm, 220 nm, and 205 nm. Increasing solvent polarity from dioxane to ethanol results in a red shift of the three bands, where the first band is shifted to 255 nm, the second band is shifted to 225 nm, and the third band is shifted to 208 nm, respectively. Furthermore, increasing solvent polarity causes a marked increase in the intensity of both bands. The three observed bands are assigned as (π–π*) transitions, based on the values of molar absorptive (ε = 70000). The interpretation of the experimentally observed UV Spectra

of **5** in dioxane and ethanol requires the theoretical calculations of the vertical transitions using CAM / B3LYP/6-311G (d, p) level. In dioxane, the band appearing in the experimental spectrum at 250 nm is reproduced theoretically using dioxane as a solvent at 247 nm (state I), as shown in Table 10, which involves orbital's φ_{53} and φ_{55}, showing a good agreement between the observed wavelength with the calculated wavelength. Theoretical gas phase calculations of compound **5** give a vertical excitation at 245 nm (state I), where the transition in the gas phase also involves the same orbital's. Increasing

Table 9. Theoretical and experimental UV spectra of **4**, calculated at CAM -B3LYP/6–311G (d, p)

	TD-Theoretical												Experimental	
	Gas phase				Dioxane				Ethanol				Dioxane	Ethanol
state	Configuration	Coefficient	f	λ, nm	Configuration	Coefficient	f	λ, nm	Configuration	Coefficient	f	λ, nm	λ_{nm}	λ_{nm}
I	58->63 58->64 60->63 62->63 62->64	-0.12 -0.14 0.20 0.24 0.58	0.181	246	59->63 59->64 60->63 62->63 62->64	0.12- -0.15 0.18 0.22 0.59	0.262	248	59->64 60->63 62->63 62->64	-0.16 0.22 0.20 0.59	0.233	247	250	255
II	58->63 60->63 60->64 62->64 62->65	0.23 0.61 -0.13 -0.15 -0.13	0.301	217	59->63 60->63 60->64 62->64	0.17 0.62 -.0.16 -0.15	0.482	219	59->63 59->64 60->63 60->64 62->64	0.14 0.12 0.63 -0.12 -0.19	0.553	220	223	226
III	58-> 63 58->64 60->63 60->64 60->65 62->64 62->65	0.19 0.44 -0.21 -0.22 -0.11 0.14 -0.31	0.181	201	59->63 59->64 60->63 62->63 62->65 62->67	0.48 -0.38 -0.11 -0.11 -0.18 -0.15	0.112	203	59->63 59->64 60->64 60->65 62->63 62->65	0.32 0.12 0.48 -0.13 0.21 0.26	0.153	202	205	208
IV	56->63 60->64 62->65	0.12 0.48 -0.47	0.391	193	59-> 63 59->64 60->64 60->65 62->63 62->65	0.38 0.13 0.43 -0.14 0.22 0.24	0.142	199	59->63 59->64 60->63 60->64 62->64 62->65 62->67	0.24 0.47 -0.16 -0.21 0.15 -0.24 0.11	0.213	198		
V	58->64 61->65 62->66 62->67 60->64	0.14 0.49 -0.36 0.55 0.94	0.401	195	59->63 59->64 60->63 60->64 60->65 62->64 62->65	0.20 0.46 -0.18 -0.19 -0.11 0.14 -0.32	0.252	193	59->63 60->64 62->64 62->65	0.12 -0.37 0.10 0.55	0.323	194		
VI	58->63 61->64 62->65 60->66	0.15 0.68 -0.77 0.32	0.251	180	56->63 56->64 59->64 60->64 60->65 62->64 62->67	-0.18 0.17 0.24 0.11 0.53 0.15 -0.14	0.13	179	56->63 56->64 59->64 60->64 60->65 62->64 62->67	-0.17 0.14 0.26 0.10 0.52 0.15 -0.17	0.12	179		

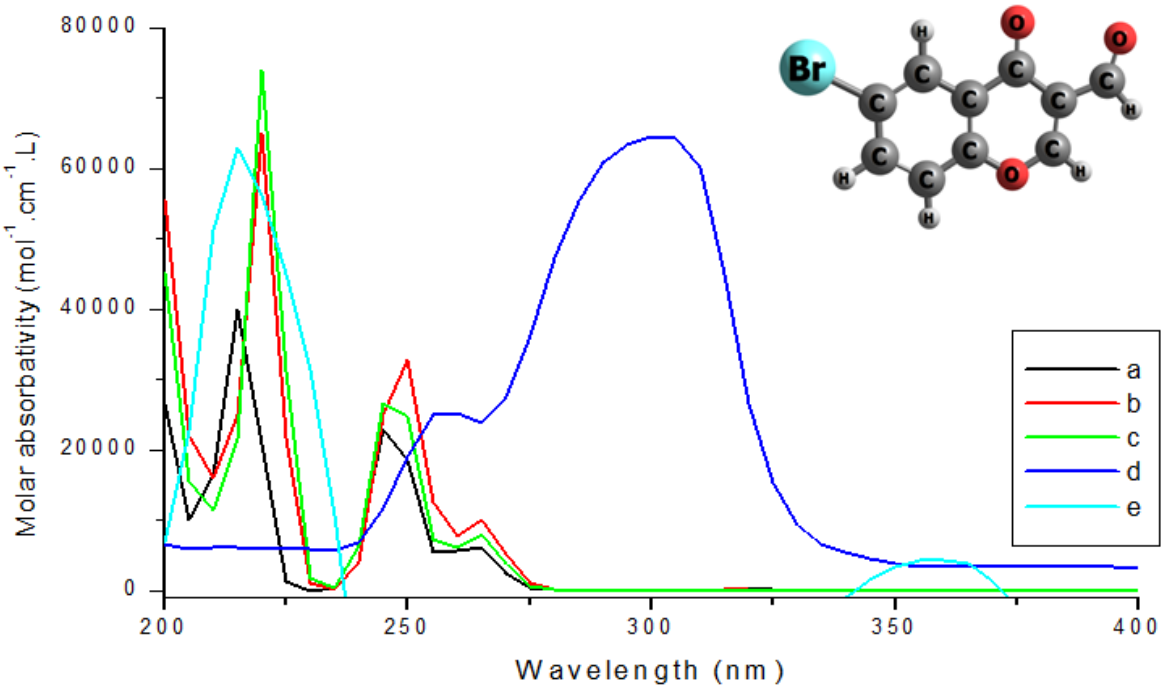

Fig. 8. Electronic absorption spectra of **4**, (a) theoretical in gas phase, (b) theoretical in dioxane, (c) theoretical in, ethanol (d) experimental in dioxane, (e) experimental in ethanol.

solvent polarity results in a red shift of λ_{max} of this band to 255 nm. The theoretical calculations of the vertical excitation in ethanol reproduce the wavelength of this band at 246 nm (state I), indicating that the same orbital's are involved in this transition. It is also clear that the calculated wave length is lower than the observed wavelength. The second band observed experimentally in dioxane at 220 nm, is reproduced theoretically at 217 nm (state II), indicating that the orbital's φ_{51} and φ_{54} are involved in this transition. Theoretical gas phase calculations give a wavelength at 215 nm (state II). This same band is observed at 225 nm in ethanol, where theoretical calculations in ethanol reproduces this band at 216 nm (state II), which is lower than the observed wavelength, where the orbital's φ_{51} and φ_{54} are involved in this transition. The third $(\pi\text{-}\pi^*)^1$ state observed experimentally at 205 nm in dioxane, is reproduced theoretically at 201 nm (state III), which involves the orbital's φ_{51} and $\varphi_{55,}$ in the transition. The gas phase calculation gives a wavelength at 200 nm (state III). In ethanol, this same band appears experimentally at 208 nm, is reproduced theoretically at 202 nm, (state III), as shown in Table 10. The fourth and five $(\pi\text{-}\pi^*)^1$ state theoretically at 197 and 177 nm in dioxane, respectively, (state IV and V). The gas phase calculation gives a wavelength at 195 and 175 nm, respectively, in ethanol, this same band appears theoretically at 196 and 177 nm respectively, as shown in Table 10. The nature of the electronic transition can be inferred from examining the electron density contours of molecular orbitals. The eight orbital's $\varphi_{49} - \varphi_{56}$, involved in the theoretical transitions of **5**, are shown in Fig. 11, show a localization and delocalization of electron density, and Charge Transfer CT character.

The results of NBO analysis of compound **5** tabulated in Table 5 indicate that there is a strong hyper conjugative interactions π^*C_3-$C_4 \rightarrow \pi^*C_9$-O_{14}, LP (2) $O_{15} \rightarrow \pi^*$ C_3-C_4, and LP (3) $Cl_{19} \rightarrow \sigma^*C_5$-$C_6$, for **5** is 127.73, 25.03, and 13.43 kcal/mol, respectively. NBO analysis of the Cl derivative Table 5 indicates that it retained the extended conjugation of **1** as revealed by the interaction of C– Cl NBOs with those of phenyl ring. Furthermore, the interaction of the cholor lone orbital's with the C5–C6 σ*orbital is marked. The population of the NBO LP (2) O_{15}, and C3–C4 reflecting a charge transfer away from the 3-fromyl-chromone ring.

Table 10. Theoretical and experimental UV spectra of **5**, calculated at CAM -B3LYP/6–311G (d, p)

	TD-Theoretical												Experimental	
	Gas phase				Dioxane				Ethanol				Dioxane	Ethanol
state	Config uration	Coefficient	f	λ, nm	Config uration	Coefficient	f	λ, nm	Configuration	Coefficient	f	λ, nm	$\lambda_{,nm}$	$\lambda_{,nm}$
I	49->54 51->54 53->54 53->55	0.14 0.18 0.24 0.59	0.171	245	49->54 49->55 51->54 53->54 53->55	0.13 0.11 0.17 0.22 0.60	0.242	247	50->54 50->55 51->54 53->54 53->55	0.10 0.12 0.21 0.20 0.60	0.213	246	250	255
II	49->55 51->54 53->55 53->56	-0.12 0.64 -0.17 -0.13	0.301	215	49->55 51->54 51->55 53->55	-0.11 0.64 -0.14 -0.16	0.472	217	50->55 51->54 53->55	0.14- 0.64 -0.20	0.543	216	220	225
III	49->54 49->55 51->54 51->55 51->56 53->55 53->56	0.23 0.47 0.17 0.27 0.16 0.11 -0.19	0.151	200	49->54 51->55 51->56 53->54 53->56	-0.41 0.43 -0.13 0.18 0.25	0.152	201	50->54 51->55 51->56 53->54 53->56	-0.36 0.47 -0.12 0.19 0.25	0.153	202	205	208
IV	51->55 53->56	0.46 -0.51	0.491	195	49->54 49->55 51->54 51->55 51->56 53->55 53->56 53->57	0.24 0.49 0.16 0.21 0.15 -0.12 0.23 -0.15	0.232	197	50->54 50->55 51->54 51->55 51->56 53->55 53->56 53->57	0.26 0.48 0.14 0.26 0.16 -0.14 0.14 -0.12	0.193	196		
V	49->55 51->56 53->55 53->57	-0.26 0.56 0.16 0.20	0.171	175	49-> 55 51->55 51->56 53->55 53->57	-0.26 0.12 0.59 0.15 -0.14	0.252	177	50-> 55 51->55 51->56 53->55 53->57	-0.29 0.10 0.56 0.15 -0.18	0.213	177		

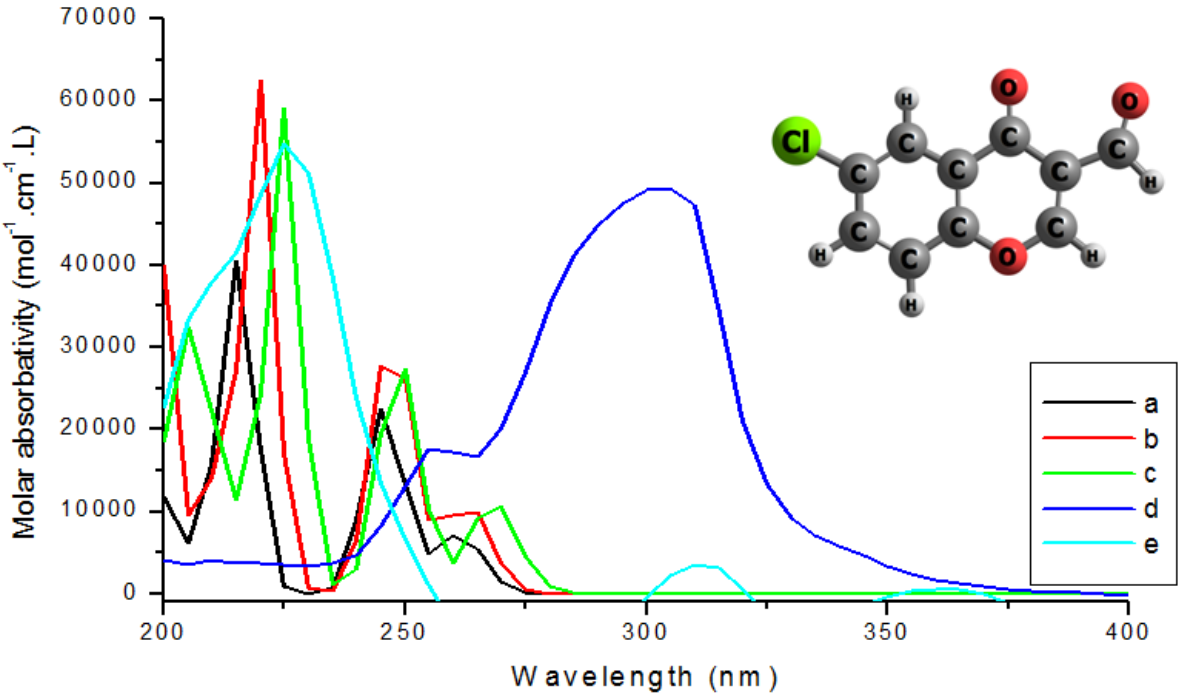

Fig. 9. Electronic absorption spectra of **5**, (a) theoretical in gas phase, (b) theoretical in dioxane, (c) theoretical in, ethanol (d) experimental in dioxane, (e) experimental in ethanol.

Electronic absorption spectra of compound 6

To complete our investigation of substituent effect on the electronic structure and spectra of compound **1**, we introduce di-Cl-atoms in position X and Y in Ph-X-Y of compound **1** gives compound **6.** The experimental and theoretical electronic absorption spectra of compound **6** in dioxane and ethanol are shown in Fig. 10 and Table 11. The experimental spectrum in dioxane is composed of three bands at 252 nm, 225 nm, and 205 nm. The change of solvent polarity from dioxane to ethanol results in a red shift of the three bands, where the first band is shifted to 256 nm, the second band is shifted to 229 nm, and the third band is shifted to 210 nm, respectively. Furthermore, increasing solvent polarity causes a marked increase in the intensity of both bands. The values of molar absorptive (ε = 60000) indicates that the three observed bands have π–π^* character. Theoretical transitions in the gas phase give a vertical excitation at 248 nm (state I), which is about 4 nm lower than the experimental wavelength, where it involves the same orbitals as in dioxane. Theoretical vertical excitation calculations in ethanol give λ_{max} of this band at 248 nm (state I), which shows agreement, implying that the orbitals involved in this transition are φ_{61} and φ_{63}. The experimental second band observed at 225 nm in dioxane, is reproduced theoretically at 223 nm (state II), where the calculations in dioxane indicate that the orbital's φ_{59} and φ_{62} are involved in this transition. Gas phase calculations give λ_{max} at 222 nm (state II). Theoretical calculations in ethanol show that, this band appears at 224 nm (state II), which is lower than the experimental wavelength. The third $(\pi\text{-}\pi^*)^1$ state observed experimentally at 205 nm in dioxane, is reproduced theoretically at 202 nm (state III), which involves the orbital's

φ_{57} and $\varphi_{62,}$ in the transition. The gas phase calculation gives a wavelength at 201 nm (state III). In ethanol, this same band appears experimentally at 210 nm, is reproduced theoretically at 203 nm, (state III), as shown in Table 11. The fourth, five, and six $(\pi\text{-}\pi^*)^1$ state theoretically at 198, 194, and 182 nm in dioxane, respectively, (state IV, V, and VI). The gas phase calculation gives a wavelength at 196, 193, and 180 nm respectively, in ethanol, this same band appears theoretically at 197, 193, and 182 nm respectively, as shown in Table 11. The nature of the electronic transition can be inferred from examining the electron density contours of molecular orbital's. The eight orbital's $\varphi_{57} - \varphi_{64}$, involved in the theoretical transitions of **6**, are shown in Fig. 11, show a localization and delocalization of electron density, and Charge Transfer CT character.

Table 11: Theoretical and experimental UV spectra of **6**, calculated at CAM -B3LYP/6–311G (d, p)

	TD-Theoretical												Experimental	
	Gas phase				Dioxane				Ethanol				Dioxane	Ethanol
state	Config uration	Coefficient	f	λ, nm	Config uration	Coefficient	f	λ, nm	Configuration	Coefficient	f	λ, nm	$\lambda_{,nm}$	$\lambda_{,nm}$
I	57-> 62 59->62 59->63 61->62 61->63	-0.16 0.17 0.13 0.24- 0.58	0.171	248	57 ->62 59->62 59->63 61->62 61->63	0.15 -0.15 0.11 0.22 0.60.	0.252	249	58->62 59->62 59->63 61->62 61->63	0.14 -0.19 0.11 0.20 0.59	0.213	248	252	256
II	57-> 63 59->62 61->63	-0.10 0.66 0.18	0.261	222	57-> 63 59->62 61->63	0.10 0.66 0.17	0.392	223	58->63 59->62 61->63	0.11 0.65 0.20	0.443	224	225	229
III	57-> 62 57->63 59->63 61->62 61->63 61->64	0.53 -0.13 -0.32 0.13 0.17 0.17	0.201	201	57-> 62 59->63 61->62 61->63	0.52 0.39 -0.14 -0.14	0.282	202	58->62 59->63 59->64 61->62 61->63	0.47 0.43 -0.12 -0.15 0.15-	0.253	203	205	210
IV	57->62 57->63 59->62 59-> 64 61->64	0.18- -0.28 -0.12 0.12- 0.57	0.281	196	57-> 62 57->63 59->62 59->66 61->64	0.12 0.34 -0.11 -0.10 0.57	0.182	198	58->62 58->63 59->62 59->66 61->64	0.12 0.36 -0.11 0.11- 0.55	0.163	197		
V	57-> 62 57->63 59->63 59->64 61->64 61->66	0.18 0.45 0.32 0.13 0.29 0.12	0.211	193	57->62 57->63 59->63 61->64 61->66	020 0.43 -0.29 -0.35 -0.13	0.292	194	58->62 58->63 59->63 61->64 61->66	0.19 0.41 -0.31 -0.37 -0.13	0.283	193		
VI	55->62 57->63 57->64 59->63 59->64 61->63	-0.11 -0.23 0.13 0.12 0.58 -0.15	0.391	180	55->62 57->63 59->63 59->64 59->66 61->63	-0.13 0.19 0.15 0.60 0.10 -0.13	0.481	182	55->62 58->63 59->63 59->63 59->64 59->64 59->64 61->63	-0.13 0.22 0.15 0.59 0.11- -0.14 0.15 -0.11	0.443	182		

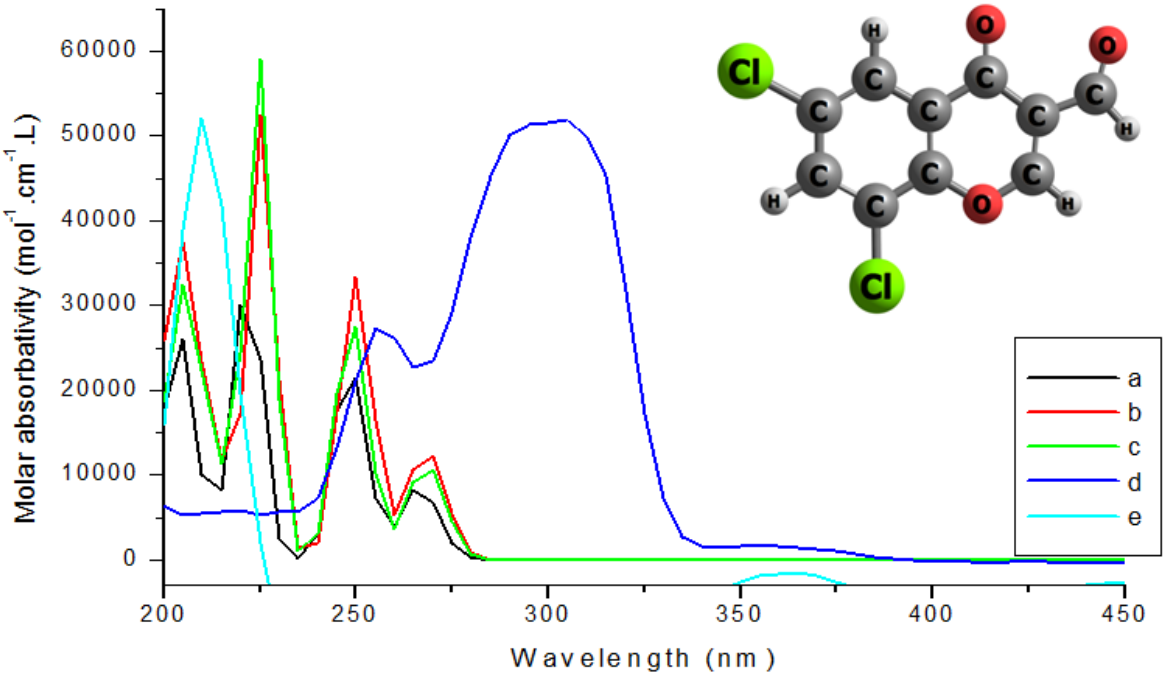

Fig. 10. Electronic absorption spectra of **6**, (a) theoretical in gas phase, (b) theoretical in dioxane, (c) theoretical in, ethanol (d) experimental in dioxane, (e) experimental in ethanol.

The results of NBO analysis of compound **6** tabulated in Table 5 indicate that there is a strong hyper conjugative interactions π^*C_3-$C_4 \rightarrow \pi^*C_8$-O_{13}, LP (2) $O_{14} \rightarrow \pi^*C_{10}$- C_{11} and πC_2-$Cl_{18} \rightarrow \pi^*C_3$-$C_4$, for **6** is 103.62, 33.71, and 26.43 kcal/mol, respectively. NBO analysis of the diCH3 derivative Table 5 indicates that it retained the extended conjugation of **1** as revealed by the interaction of C– Cl NBOs with those of phenyl ring. Furthermore, the interaction of the cholor lone orbital's with the C5–C6 σ*orbital is marked. The population of the NBO C1–C2, LP (2) O_{14}, and C3–C4 reflecting a charge transfer away from the 3-fromyl-chromone ring.

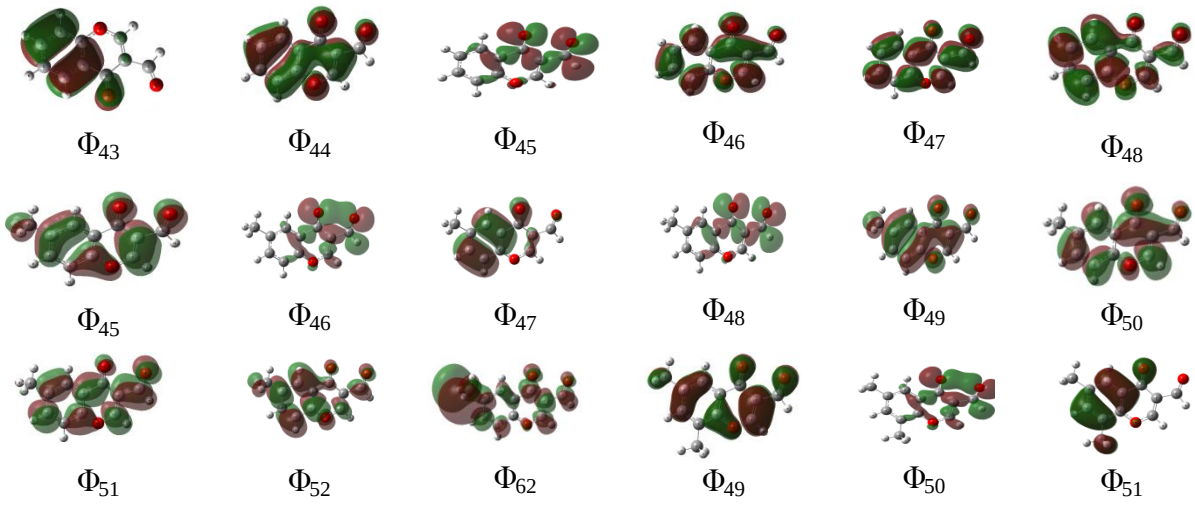

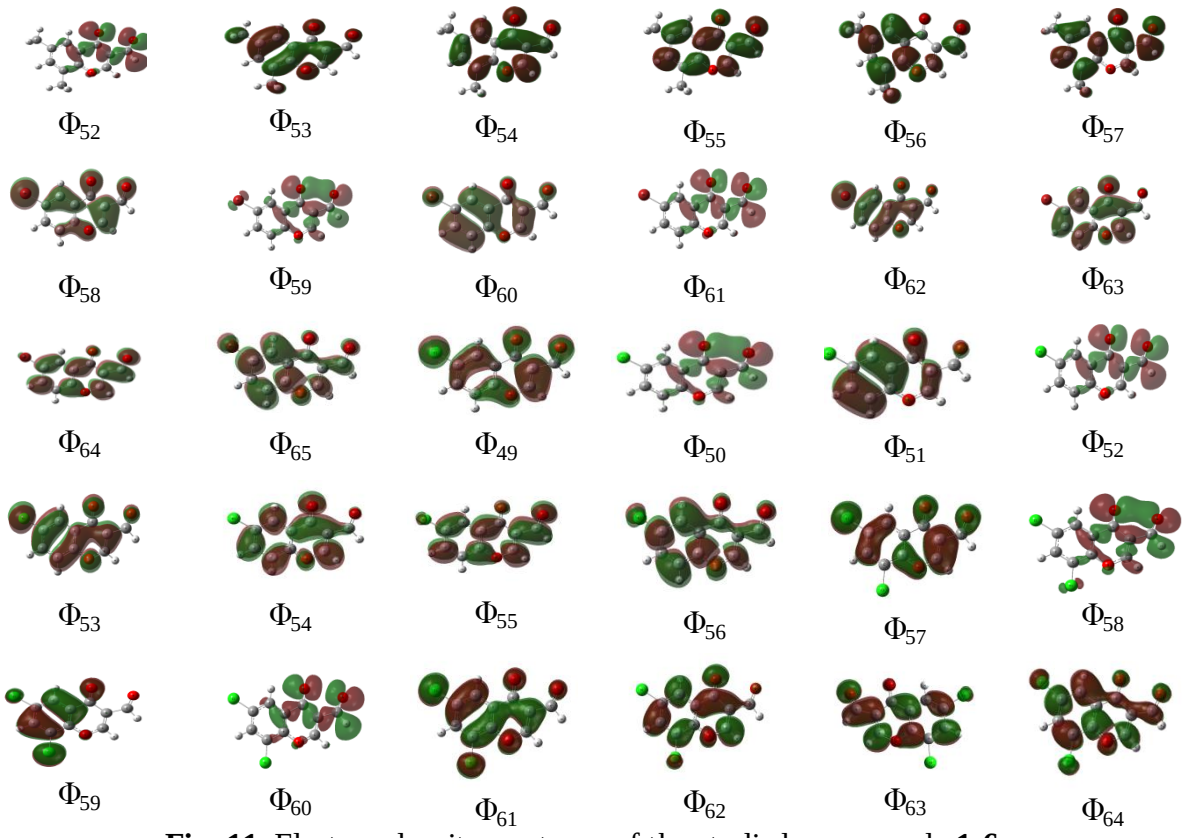

Fig. 11. Electron density contours of the studied compounds **1-6**.

Biological activity

The biological activity of the studied compounds **(1-6)** was tested against Grame positive bacteria, Grame negative bacteria with Gentamycin and Fungi with Ketoconazole as standard reference for each respectively as shown in Table 12 and Fig. 12. Concerning Grame positive bacteria, two types of bacteria were used in the testing procedure, which are S.aureus and B.subtillis. The compound **3** was less to moderate biologically active compared to standard reference, while the substituted compounds showed different biological activity. Compound **6** was moderately active compared to the parent and the substituted compounds (**5, 4, 1** and **2**) were highly active than the parent compound **1**. Concerning Grame negative bacteria, two types of bacteria were also used in the testing procedure, which are S.typhimurium and E.coli. The compound **3** showed less to moderate biological activity compared to standard reference. On the other hand, the substituted compounds showed variations in the biological response, Compound **6** was highly active compared to the parent compound **1,** while the substituted compounds (**5, 2, 4** and **1**) were moderately active compared to the parent. Moving to Fungi, C.albicans and A.fumigates Thom were the two types used in the testing procedure. The compound **3** showed less to moderate biological activity compared to standard reference. All the substituted compounds (**6, 5, 4, 2** and **1**) showed moderate in the biological activity compared to the parent.

The studied compounds can be arranged according to their biological activity against Grame positive bacteria, Grame

negative bacteria and Fungi compared to standard reference as follows: Compound **6,** comes first with the highest biological activity, than compound **5**, this is followed by **4, 1, 2** and the compound **3,** is the last one with the least biological activity i.e. **6 > 5 > 4 > 1 > 2 > 3.**

Table 12. Antimicrobial Activity for the studied compounds **1-6**.

compounds	Diameter of inhibition zone (mm) at conc. of (µg/ml)					
	Grame +Ve		Grame -Ve		Fungus	
	S.aureus	B.subtillis	S.typhimurium	E.coli	C.albicans	A.fumigates
1	18	17	14	27	27	30
2	14	15	17	22	31	30
3	12	14	14	18	31	35
4	19	18	14	28	25	28
5	22	19	17	29	25	26
6	22	20	20	29	22	20
Gentamycin[a]	24	26	17	30	-----	-----
Ketoconazole[b]	---	----	-----	------	20	17

[a] Antibacterial standard.
[b] Antifungal standard.

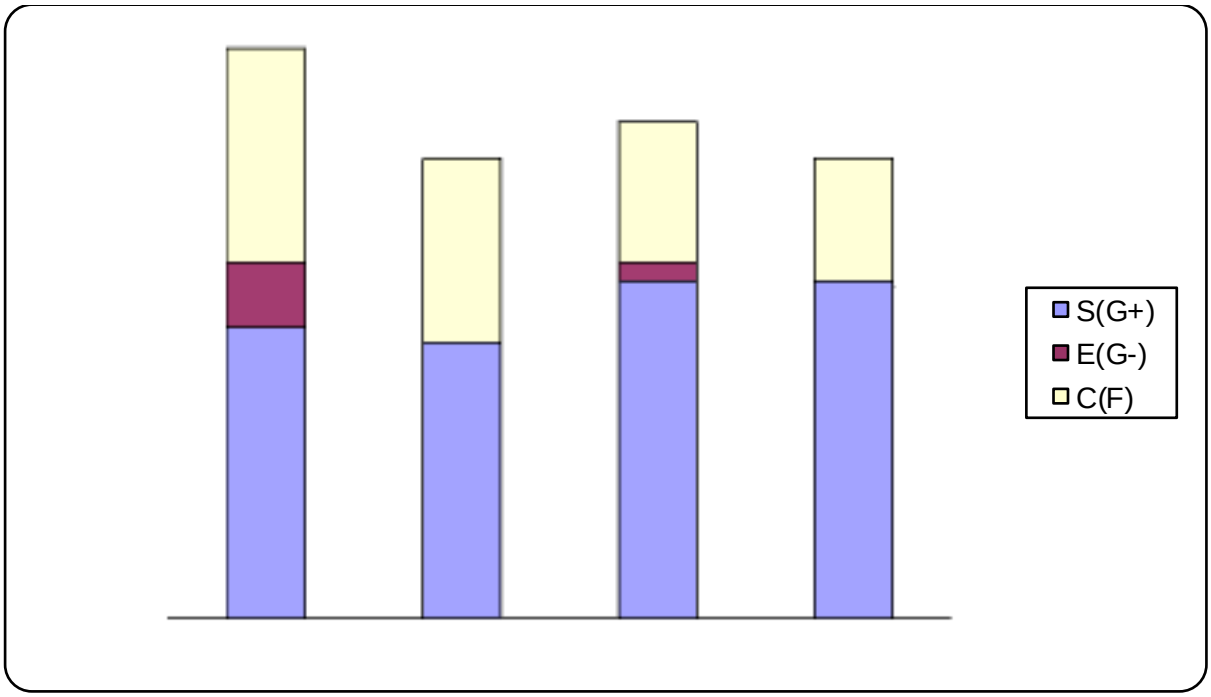

Fig. 12. Antimicrobial activity for the studied compounds **1-6** against gram-positive bacteria (G^+), gram-negative bacteria (G^-), and Fungi (F).

Correlation between biological and ground state properties

The biological activity of the studied compounds can be correlated with the ground state energetic and global properties. From the computed data in (Table 3), one can reveal the following: The biological activity of the studied

compound obtained experimentally follow the order **6 > 5 > 4 > 1 > 2 > 3**, Against G+, G- and fungi. The theoretical chemical reactivity, Eg, of the studied compound computed at B3LYP/6-311G (d,p) follow the same order obtained experimentally indicating that Eg is one factor contributing to the reactivity of the studied compounds (c.f. Table 3). The theoretically computed chemical hardness (η) and electronegativity (χ), chemical potential (V), and natural charge from NBO of the studied compounds follow the same order of the experimental biological activity which is **6 > 5 > 4 > 1 > 2 > 3**. Whereas, the global softness (S), and global electrophilicity index, (ω), follow the reverse order of the experimental biological activity **3 > 2 > 1 > 4 > 5 > 6.** In case of the mean first-order hyperpolarizability (β), the order are **1 > 2 > 3 > 5 > 4 > 6** which violate the order of the experimental biological activity.

SUMMARY AND CONCLUSION

Electronic structure of chromone-3-carboxaldehyde, compound **1** and its derivatives, **2–6**, are investigated theoretically at B3LYP/6-311G (d, p). All the studied compounds are found to be planar. The ground state properties of **1** and its derivatives show that compound **6** has the lowest E_{HOMO}, E_{LUMO}, and E_{gap} indicating highest reactivity. From the computed dipole moment, compound **3** is found to have the highest polarity. Mullikan and natural charge distribution of the compounds **1–6** were studied which indicated the electronic charge distribution. The calculated dipole moment and first order hyperpolarizability results indicate that the molecule has a reasonable good non-linear optical behavior. MEP confirmed the different negative and positive potential sites of the molecule in accordance with the total electron density surface. Electronic absorption spectra are investigated experimentally in dioxane and ethanol; and theoretically in gas phase, dioxane and ethanol using CAM-B3LYP/6-311G (d, p). Compounds **1–6** exhibit 7 bands. The band maxima (λ_{max}) and intensities of the spectra are found to have solvent dependence. The bands of compounds **1, 2,** and **3** show blue shift, while compounds **4, 5** and **6** show red shift. Theoretical calculations of the vertical excitations at the CAM-B3LYP/6-311G (d, p) reproduce the experimental spectra, indicating a good agreement between theory and experiment. The NBO analysis of the compounds **1–6** indicated the intermolecular charge transfer between the bonding and antibonding orbital's. The biological activity of the studied compounds show that compound **6** (**di-Cl**) is the most active one ,whereas, the molecule **3** (**di-CH3**) is the least active and the order of reactivity is **6 > 5 > 4 > 1 > 2 > 3.**

ACKNOWLEDGEMENTS

This work was supported by the preparation of 3-fromyl-chromone derivatives compounds by Dr. Magdy. A. Ibrahim at the Faculty of Education, Ain Shams University, Roxy 11711, Cairo, Egypt **Conflicts of interest:** The Manuscript that do not include a conflict of interest, and so there is no funded entity for this research**.**

REFERENCES

[1]. R. S. Keri, S. Budagumpi, R. K. Pai, R.G. Balakrishna, Eur. J. Med. Chem. 78 (2014) 340-374.

[2]. A. Rampa, L. Piazzi, F. Belluti, S. Gobbi, A. Bisi, M. Bartolini, V. Andrisano, V. Cavrini, A. Cavalli, M. Recanatini, P. Valenti, J. Med. Chem. 44 (2001) 3810-3820.

[3]. J. Schmitz Francis, Jong Hwan Kwak, and Michelle Kelly, J. Nat. Prod. 63 (2000) 1153-1156.
[4]. Y. Q. Shi, T. Fukai, H. Sakagami, W. J. Chang, P. Q. Yang, F. P. Wang, T. Nomura, J. Nat. Prod. 64 (2001) 181-188.
[5]. Q. Chen, X. L. Zhu, L. L. Jiang, Z. M. Liu, G. F. Yang, Eur. J. Med. Chem. 43 (2008) 595-603.
[6]. W. Huang, Q. Chen, W. C. Yang, G. F. Yang, Eur. J. Med. Chem. 66 (2013) 161 - 170.
[7]. R. Larget, B. Lockhart, P. Renard, M. Largeron, Bioorg. Med. Chem. Lett. 10 (2000) 835-838.
[8]. J. Ungwitayatorn, W. Samee, J. Pimthon, J. Mol. Struct. 689 (2004) 99-106.
[9]. Ibrahim Magdy. J. Synthetic Communications 39 (2009) 3527-3545.
[10]. Santosh Kumar and Joonseok Koh, Int. J. Mol. Sci. 13 (2012) 6102-6116.
[11]. R. Raja, S. Kandhasamy, P. T. Perumal, A. SubbiahPandi, Acta. Cryst. E71 (2015) 0512-0513.
[12]. P. J. Pietta, J. Nat. Prod. 63 (2000) 1035-1042.
[13]. M. Mazzei, E. Sottofattori, R. Dondero, M. Ibrahim, E. Melloni, M. Michetti, Farmaco 54 (1999) 452-460.
[14]. F. Albericio, H. G. Kruger, Future. Med. Chem. 4 (2012) 1527-1531.
[15]. G. Singh, R. Singh, N. K. Girdhar, M. P. S. Ishar, Tetrahedron 58 (2002) 2471-2480.
[16]. C. Chang, C. Wu, S. Kuo, J. Wang, C. Teng, Chin. Pharm. J. 54 (2002) 127-140.
[17]. Sung Hwan Kim, Sangku Lee, Se Hee Kim, and Jae Nyoung Kim. Bull. Korean. Chem. Soc. 29 (2008) 1815-1818.
[18]. Su-Moon Park and Hyo Joong Lee. Bull. Korean Chem. Soc. 26 (2005) 697-706.
[19]. A. M. Farag, A. Magdy Ibrahim, M. Nasser El-Gohary, N. Roushdy, Arabian Journal of Chemistry. In Press (2016).
[20]. L.E. Lawrence, M. J. Pucci, M. Frosco, J. F. Barrett, Expert Opin Investig Drugs. 8 (1999) 2201-2223.
[21]. H. M. Hosni, M. M. Abdulla, Acta Pharm. 58 (2008) 175-186.
[22]. Z. N. Siddiqui, S. Praveen. F. Farooq, Chem. Pap. 64 (2010) 818-824.
[23]. M. A. M. Ibrahim, Eur. J. Chem. 1 (2010) 124-128.
[24]. S. S. Ibrahim, H. A. Allimony, A. M. Abdel-Halim, M. A. Ibrahim, Arkivoc xiv (2009) 28-38. ISSN 1551-7012.
[25]. Z. N. Siddiqui, Tetrahedron Lett. 53 (2012) 4974-4978.
[26]. S. Abdel Halim, Ali Kh. Khalil, J. Mol. Struct. 1147 (2017) 651-667.
[27]. S. Abdel Halim, M. A. Ibrahim, J. Mol. Struct. 1130 (2017) 543-558.
[28]. S. Abdel Halim, Laila I. Ali, Sameh Gamal Sanad, Int. J. Nano Dimens., 8 (2017) 142-158.
[29]. A. D. Becke, J. Chem. Phys. 98 (1993) 5648-5652. (b) A. D. Becke J. Chem. Phys. 98 (1993) 1372-1376.
[30]. C. Lee, W. Yang W, R. G. Parr, Phys. Rev. B Condens. Matter. 37 (1988) 785-789.
[31]. Stefanov, B. G. Liu, A. Liashenko, P. Piskorz, I. Komaromi, R. L. Martin, D. J. Fox, T. Keith, M. A. Al-Laham, C. Y. Peng, A. Nanayakkara, M. Challacombe, P. M. W. Gill, B. Johnson, W. Chen, M. W. Wong, C. Gonzalez, J. A. Pople, Gaussian, Inc., Pittsburgh PA. (2003).
[32]. M. Frisch, J. G. W. Trucks, H. B. Schlegel, G, E. Scuseria, et al., Gaussian, Inc., Wallingford CT, (2009).

[33]. GaussView, Version 5, Dennington, R.; Keith, T.; Millam, J. Semichem Inc., Shawnee Mission KS, (2009).
[34]. http://www.chemcraftprog.com.
[35]. D. Avci, Spectrochim. Acta A. 82 (2011) 37-43.
[36]. D. Avci, A. Başoğlu A, Y. Atalay, J. Chem. Article ID 712130 (2013) 1-16.
[37]. S. Tomasz, S. Katarzyna S, C. Benoît, J. Chem. Phys. 141(2014) 104109.
[38]. R. G. Pearson, Proc. Nat. Acad. Sci. 83 (1986) 8440-8441.
[39]. K. Chandra, and T. Uchimara, J. Phys. Chem. A. 105 (2001) 3578 - 3582.
[40]. Nicolas Clavier, Renaud Podor, Nicolas Dacheux, J. Europ. Cera. Soc. 31 (2011) 941-976.
[41]. T. Yanai, D. Tew, and N. Handy, Chem. Phys. Lett. 393 (2004) 51-57.
[42]. [42] J. Chocholoušová, V. Špirko, P. Hobza, Phys. Chem. Chem. Phys. 6 (2004) 37-41.
[43]. M. Szafran, A. Komasa, E. Bartoszak-Adamska, J. Mol. Struct. 827 (2007) 101-107.
[44]. D. John Mitchell, and W. Barry Ninham, J. Chem. Soc. Farady Trans. II, 77 (1981) 601-629.
[45]. D. Sajan, L. Joseph, N. Vijayan, M. Karabacak, Spectrochim. Acta A. 81 (2011) 85-98.
[46]. C. Reddy, D. Rao, V. Yakub, A. Nagaraj, Acta Chim. Slov. 57 (2010) 798-807.
[47]. S. Natorajan, G. Shanmugam, and S. A. MartinCryst, Technal. 43 (2008) 561; D. S. Chemia, J. Zysss, (1987) Nonlinear Optical Properties of Organic Molecules and Crystals Academic Press, F. L. Orlando, D. S. Bradshow, D. L. Andrews, J. Nonlinear Opt. Phys. Matter 18 (2009) 285. S. Sures (2013) Single Crystal Scientific-Research An Academic Publisher1, 3 (2013) 87-91.
[48]. L. T. Cheng, W. Tam, S. H. Stevenson, G. R. Meredith, G. Rikken, S. R. Marder, J. Phys. Chem. 95 (1991) 10631.
[49]. P. Kaatz, E. A. Donley, D. P. Shelton, J. Chem. Phys. 108 (1998) 849-855.
[50]. T. Gnanasambandan, S. Gunasekaran, S. Seshadri, Spectrochimica. Acta Part A: Molecular and Biomolecular Spectroscopy 117 (2014) 557-567.
[51]. J. S. Murray, K. Sen, Molecular Electrostatic Potentials, Conseptsana Applications, Elsevier, Amsterdam 7 and Sscrocco E, Tomasi J, (1978) Electronic Molecular Structure, Reactivity and Intermolecular Forces: An Euristic Interpretation by Means of Electrostatic Molecular Potentials, Adv. Quant. Chem. 11(1996) 115-193.
[52]. P. Politzer, J. S. Murray, Theor. Chem. Acc. 108 (2002) 134-142.
[53]. D. Sajan, L. Joseph, N. Vijayan, M. Karabacak, Spectrochim. Acta A. 81 (2011) 85-98.